NASA / DLR Aeronautics Design Challenge 2018

RosE

by

D. Adamik, V. Dingelmaier, A. Jastrzebska, T. Klotzsche, A. Rahn, L. Sano, M. Trapp

Team Members

Team members from left to right:

Martin Trapp
Aeronautical Engineering

Antonia Rahn
Aeronautical Engineering

Viktor Dingelmaier
Aerospace Engineering

Lion Sano
Aerospace Engineering

Tim Klotzsche
Aeronautical Engineering

Agnieszka Jastrzebska
Aeronautical Engineering

David Adamik
Aeronautical Engineering

Academic Support
Dipl.-Ing. Florian Dexl
Chair of Aircraft Engineering
TU Dresden

RosE
electric • eco-friendly • efficient

© DDPix.de

Declaration of Authorship

We hereby declare that the thesis submitted is our own unaided work. All direct or indirect sources used are acknowledged as references.

We are aware that the thesis in digital form can be examined for the use of unauthorized aid and in order to determine whether the thesis as a whole or parts incorporated in it may be deemed as plagiarism.

This paper was not previously presented to another examination board and has not been published.

Dresden, 27.06.2018
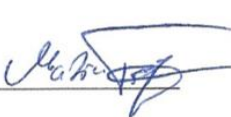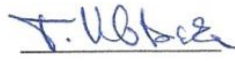
Technische Universität Dresden, 01062 Dresden

Deutsches Zentrum für Luft- und
Raumfahrt e. V. (DLR)
Institut für Systemarchitekturen in der
Luftfahrt | Flugzeugentwurf &
Systemintegration

Prof. Dr.-Ing.
Klaus Wolf
Lehrstuhl für Luftfahrzeugtechnik

Bearbeiter: Florian Dexl

Telefon: 0351 463-38096
Telefax: 0351 463-37263
E-Mail: florian.dexl@tu-dresden.de
AZ: 18-06

27/06/2018

NASA/DLR Design Challenge: Approval and support of report submission

To whom it may concern,

As the academic supervisors, we hereby declare to approve the report written by
the student team consisting of
- David Adamik,
- Viktor Dingelmaier,
- Agnieszka Jastrzebska,
- Tim Klotzsche,
- Antonia Rahn,
- Lion Sano,
- Martin Trapp

and support the submission to the NASA/DLR Design Challenge 2018.

Best regards

TECHNISCHE
UNIVERSITÄT
DRESDEN
Institut für Luft- und Raumfahrttechnik
Lehrstuhl für Luftfahrzeugtechnik
Prof. Dr.-Ing. Klaus Wolf
01062 Dresden

Prof. Dr.-Ing. K. Wolf

Dipl.-Ing Florian Dexl

Nomenclature and Indices

a_z	Centrifugal acceleration	$\dfrac{m}{s^2}$
b	Span	m
c_D	Drag coefficient	$-$
c_{D0}	Parasite drag coefficient	$-$
$c_{D,i,box}$	Drag coefficient of box-wing	$-$
$c_{D,i,ref}$	Drag coefficient of reference aircraft	$-$
c_L	Lift coefficient	$-$
c_{Wi}	Induced drag coefficient	$-$
c_{WW}	Wave drag	$-$
D	Drag	N
$D_{i,Box}$	Induced drag of box-wing	N
$D_{i,ref}$	Induced drag of reference aircraft	N
DNL	Day Night Average Sound Level	dB
E	Efficiency energy	$\dfrac{MJ}{kW}$
ΔE_{Drag}	Reduction of drag	J
$e_{Kerosene}$	Specific energy of kerosene	$\dfrac{J}{kg}$
ΔE_{Kin}	Difference of kinetic energy	J
ΔE_{Pot}	Difference of potential energy	J
E_{Prop}	Energy for propulsion	J
E_{Tank}	Energy stored in the tank	J
f_L	Approx. part of energy used for cabin, avionics, etc.	$-$
g	Standard gravity	$\dfrac{m}{s^2}$
h	Height	m
Δh	Difference of vertical height	m

h_E	Height	m
k	Factor of energy saving	—
L	Lift	N
m	Mass	kg
m_F	Mass of fuel	kg
P	Propulsive power	W
P_{eff}	Efficiency weight	$\dfrac{kg}{kW}$
R	Radius	m
s	Range	m
S_H	Elevator area	m^2
S_V	Vertical tail area	m^2
S_{V-Tail}	V-Tail area	m^2
S_W	Surface wing area	m^2
T	Thrust	N
t	Flight time	s
U	Voltage	V
v	Speed	$\dfrac{m}{s}$
v_1	Critical take-off decision speed	$\dfrac{m}{s}$
v_E	Velocity	$\dfrac{m}{s}$
Δv	Difference of speed	$\dfrac{m}{s}$
$\eta_{Turbine}$	Efficiency of a gas turbine	—
η_{FC}	Efficiencies of the fuel cells	—
η_{HTS}	Efficiencies of the motors	—
η_{Prop}	Efficiencies	—
γ	Angle between tail areas	°
ρ	Density	$\dfrac{kg}{m^3}$

θ	Inclination of runway	°
ϑ	Temperature	K

Indices

$(\dots)_{A330}$	Airbus A330
$(\dots)_{Climb}$	Climb
$(\dots)_{Cruise}$	Cruise
$(\dots)_{req}$	Required
$(\dots)_{TO}$	Take-off
$(\dots)_{Total}$	Total

Table of Contents

TABLE OF CONTENTS

1. Introduction

Air traffic has proven itself to be a great economic success and grew to a billion-dollar industry until this day. Since first commercial aircraft were put into commission, the demand for this fast and convenient means of transportation has grown continuously. Further good news for the aviation market have emerged when *IATA* revealed a forecast expecting a near doubling of passenger numbers to 7.8 billion by 2036, promising a great future for the industry [1]. While comfort, flight time and safety have been improved to a never before known level, environmental concerns have been neglected. This, in combination with the continuous rise of demand, poses a massive problem for the ecosystem as conventional aircraft emit noise and climate-damaging fumes. They are responsible for a significant part of CO_2 and NO_x in the atmosphere today.

Numerous strategies have been put into place to counter these negative effects and to push eco-friendlier air traffic, such as: Europe's Flightpath 2050 and the *NASA Aeronautics Research Mission Directorate's* (ARMD) strategic pushes being the weightiest. The *NASA/DLR Aeronautics Design Challenge 2018* keeps its requirements close to these of ARMD and demands a 60-80 % reduction in energy consumption, an 80 % cut in landing/take-off cycle (LTO) and cruise NO_x emission as well as 42-52 dB noise reduction compared to a 2005 best-in-class reference aircraft.

The following concept has been developed by seven students of the *Technische Universität Dresden* through extensive literature research, evaluation, discussion and calculation. Although several of the used technologies and materials are currently of a low technology readiness level (TRL), only those with great potential and predictability were chosen to be used for this project. To maintain credibility and to not distort the feasibility of particular improvements, compromises have been made for the researched range of possible performance enhancements.

This concept is designed for future implementation by aviation industry. The aim is an entry into service (EIS) by 2045. Though it has large-scale modifications, an immediate adaption is considered to be impossible. Thus, a step-by-step implementation of the presented technologies is suggested.

2. Project Requirements

Future economy is facing radically increasing demand for air traffic. It is expected that the amount of flights and flight passengers will increase strongly throughout the next decades. As emissions due to aviation have major impact on the environment and society, the industry has a responsibility to take countermeasures against the globally worsening ecological situation.

Top level requirement is reducing energy consumption and emission of greenhouse gasses. Around 110,000 g of carbon dioxide (CO_2) and 520 g of nitrogen oxides (NO_x) are emitted for every 1,000 passengers/kilometre in heights where the impact on the environment is the greatest [2]. Regarding a long-term goal of 25 to 30 years – in this case until 2045 – the energy consumption of future aircraft shall be reduced by at least 60 %, and emissions of mentioned gases by up to 80 %.

A further problem to deal with are noise emissions. Nowadays, around 750,000 people are bothered by aviation noise in Germany [3]. The *Federal Aviation Authority* (FAA) issued airport requirements that demand a 'Day Night Average Sound Level' (DNL) of 65 dB [4] whereas the *German Federal Environment Agency* has even prescribed a law saying that noise protection must be built for new airports exceeding 60 dB [5]. Therefore, a reduction of aircraft noise up to 52 dB is being strived for the next 30 years. The main reason for trying to accomplish these requirements is to stop or at least to slow down the effects of global warming and to maintain a healthy environment. To combine these constraints with rising demand of air traffic, rethinking the infrastructure becomes crucial.

3. Reference Aircraft

Short-range aircraft are expected to be less important by 2045 due to new developments enabling a faster transport with lower operating effort, like the *Hyperloop*. Abu Dhabi, for example, is specifying its plans to build such tracks in 2020 [6]. Furthermore, electric propulsion using hydrogen technology appears to be more efficient on long distances. Therefore, a long-range aircraft has been chosen as reference aircraft.

The *Airbus A330-200* is a twin-aisle commercial transport aircraft designed for long-range transatlantic flights. It was put into commission in April 1998 and is available with three different options of engines. These are the *General Electric CF6-80E1*, the *Pratt & Whitney PW4164/8* and the *Rolls-Royce Trent 700*. The most used engine for the *A330* is the *Rolls-Royce Trent 700* with the lowest fuel burn [7]. The aircraft's operational costs are about 25 % lower than those of the *Boeing 767-300ER* [8]. The lowest recorded fuel consumption was only 2.7 litres per passenger per 100 kilometres [9]. Compared to the *A330-300*, the *A330-200* has a lower operating empty weight (OEW), lower total drag and requires lower cruise thrust [7]. The *A330*-family is recognised for its operational reliability of over 99.4 % [9]. Furthermore, the *A330* was the first *Airbus* aircraft fitted with new navigation technologies such as the Multi-Mode Receiver (MMR). In 2003, the model's cockpit was upgraded with liquid crystal displays (LCD). Integrated standby instrument systems (ISIS), fly-by-wire rudder and a new on-board maintenance data system were installed. Those implementations represented the state of the art at that time. Due to the combination of low operating costs, high efficiency, flexibility and optimised performance, the *A330* was the best aircraft in its class in 2005 [10]. Therefore, the *A330-243* with *Rolls-Royce Trent 700* engines is the most reasonable choice as reference aircraft. Table 1 shows the specifications of the reference aircraft.

Key data fact	value	
Length	57.51	m
Wingspan	60.30	m
Height	17.39	m
Wing area	361.60	m^2
Number of engines	2	
Thrust per engine	316,000	N
Total thrust	632,000	N
Maximum take-off weight	233,000	kg
Range	10,540	km
Cruise speed	M0.82	
Typical passenger capacity	278	

Table 1: Key Data Airbus A330-243; [18] [69]

4. Technology

Based on the guidelines of chapter two, specific technological solutions are outlined in the following. In general, a blended wing body configuration has the potential to reduce noise pollution emitted by engines [11], since large wing surfaces can shield sounds. Further advantages of such a configuration are fuel saving properties, due to the fuselage itself creating additional lift and a lower empty weight. This has been developed to a preliminary concept with a short fuselage integrated in a large wing section. However, those promising advantages are opposed by severe disadvantages. A wide fuselage would have caused comfort problems at seating positions displaced more than two metres from the aircraft's longitudinal axis due to stronger g-forces. Examining *Certification Specification 25* (CS 25), this concept also would have had severe problems concerning evacuation. Since operating safety is the fundamental basis for aircraft development, this concept has been dropped.

Taking these disadvantages into account, a smaller fuselage with aerodynamically beneficial blended wings has been chosen. Due to the blending of the wing, a higher volume was achieved, offering more space to

integrate a propulsion system. The passenger cabin would have had an oval cross section making cabin pressurisation easier and an arrangement of passenger seats close to the longitudinal axis would have been possible. Evacuation would still have been complicated due to emerging huge wing sections. Realising a family concept would have been difficult and an enormous wing box would have been necessary.

Earlier mentioned contemplations lead to the conclusion that a fuselage configuration as practical as possible had to be found. The chosen *Airbus A330-200* provides a well-balanced compromise between given requirements and constraints. On one hand all effort for the fuselage's certification has already been done and on the other hand its family concept can be maintained. Additionally, the body provides a range of further advantages: passenger capacity and cargo volume remain constant; the fuselage's safety and ground handling procedures are proven.

Next, decisive factors such as wing configuration, empennage, propulsion system and infrastructure had to be rethought. Adapted from the blended wing configuration, massive wing roots, also offering structural space for the propulsion system, are used to induce lift. The wings, positioned at the original location of the fuselage, have thicker roots due to blending, a longer chord and a shorter span width using a box wing configuration. An all-electric propulsion system is installed on top of the wing, covered by the mentioned box wing configuration. A second, massive wing box for the upper wing is not necessary as the e-fans fulfil the structural support in this area, resulting in a reduced structural mass. Regarding further potential for mass reduction, the wing span was shortened, and wing panels were constructed thinner because the utilised configuration creates higher stability. The final setup was found choosing a conventional fuselage and integrating a wing structure combining blended wings at the roots and boxed wings at the tips. The approach appears to be promising to achieve optimal flight characteristics and eco-friendly developments. The design takes into consideration the passengers' safety, comfort, productional and operational costs.

Figure 1 shows the design of the new aircraft with its dimensions.
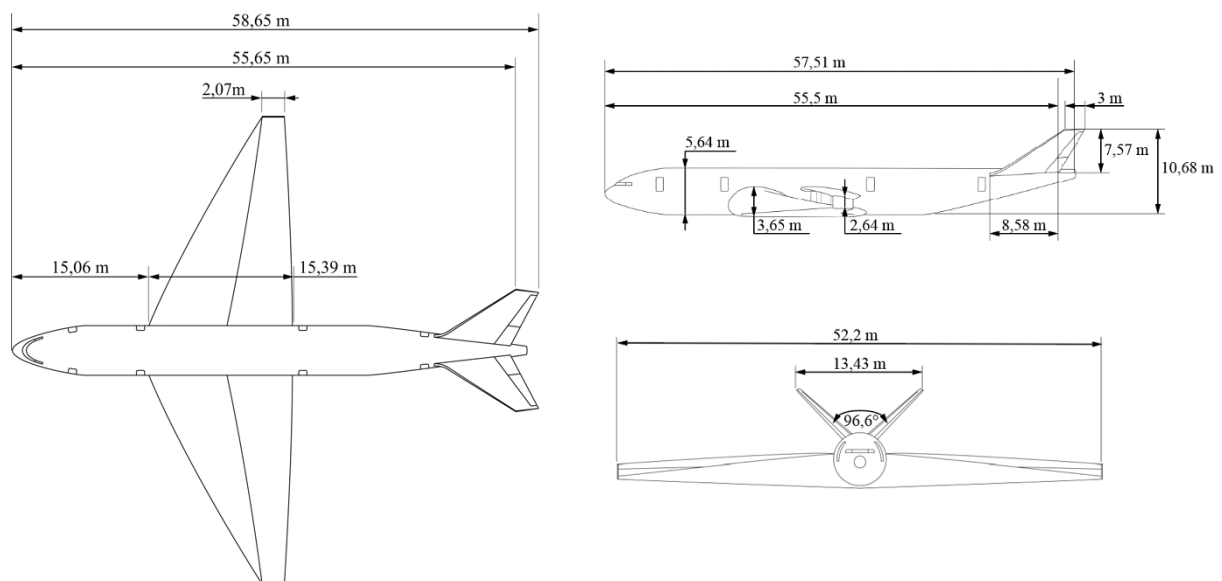
Figure 1: Three-way View

Considering current research and potential future developments, optical changes, aerodynamic aspects, material improvements as well as possible cost savings on ground are analysed. Aerodynamic progress is not only determined by the aircraft's shape but also by its surface qualities. For improved surface qualities, the so-called sharkskin can be applied at positions with high airflow. Furthermore, materials are expected to change their functionality in near future. By 2045, materials could be self-repairing which would offer tremendous possibilities in flight operations, bringing profound changes in maintenance work and costs.
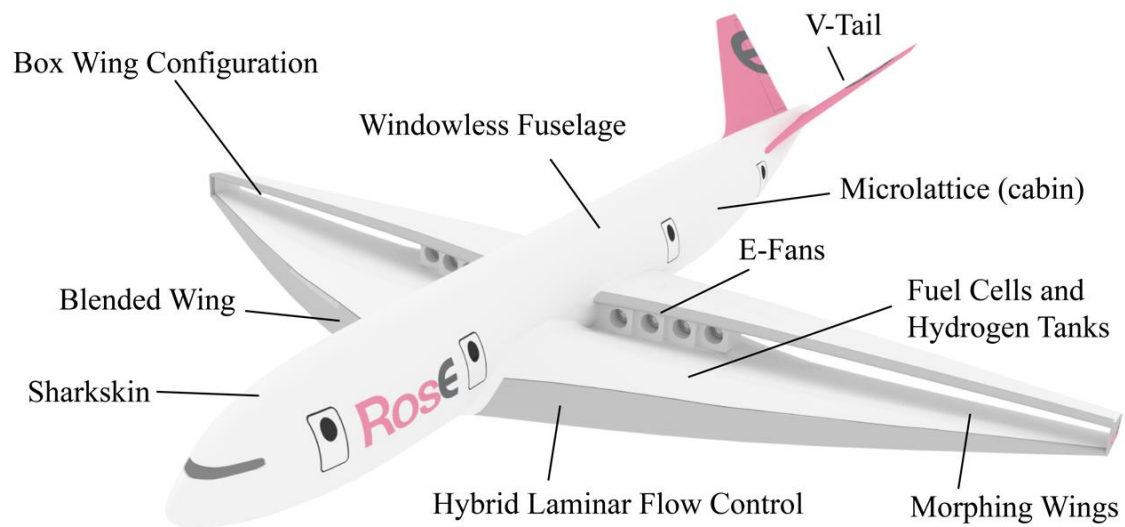
Figure 2: Key Technologies

Infrastructural adjustments complete the aircraft's concept. A completely new take-off and landing procedure will provide higher efficiency, while the airport is designed for a progressive implementation, meaning that every airport can be retrofitted stepwise.

The flower-shaped airport inspires the name of the idea: *RosE*, past tense of 'to rise', shows that an eco-friendly, all-electric and efficient concept is ready for take-off and to rise towards a new future.

5. Infrastructure

5.1. Current Deficiencies

Efficiency is the most important criterion for future infrastructure concepts. Exponential population growth to an estimated nine to ten billion by 2040 and the expected rise of passenger numbers resulting from it requires new airport concepts [12]. Efficient utilisation of building ground will become even more crucial than it is today. Examining conventional airport designs, it is obvious that the ratio of used area to total area is low. Conventional runways bring major disadvantages in matters of take-off and landing procedure, thus in logistic efficiency. Long ways to the runway delay take-off and landing. Furthermore, runways are limited in length which is critical for emergency manoeuvres. Since winds, especially their direction, have major impact on logistics and scheduling, having runways set in one or two given directions is a profound hindrance for realising fluent traffic. Therefore, in order to achieve optimal standard departure and arrival routes, to decrease power consumption and to optimise the traffic flow simultaneously, improving the infrastructure is fundamental.

5.2. Design

A circular airport design as shown in figure 3 is chosen, consisting of the following components: centralised terminal facilities, tower and apron, outer circular runway and the connection between runway and apron, which we call arms. These connections are tangent to the runway.
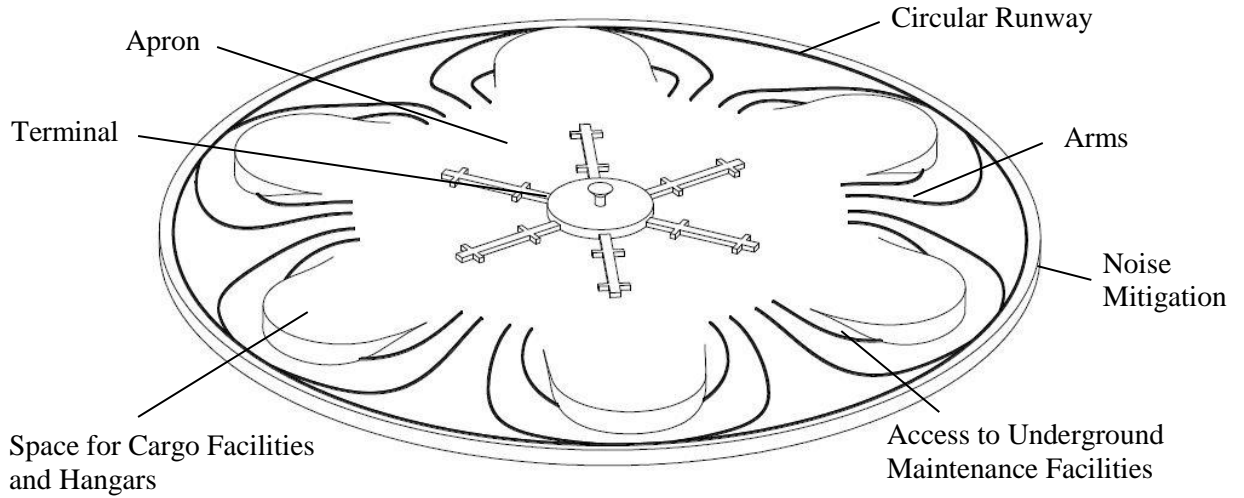
Figure 3: Airport Schematic Diagram

The airport has a diameter of 3 km and a total area of 7.07 km². An elevated apron with a diameter of 840 m results in an apron area of 0.54 km². There are 48 airbridges, each leading to a parking position of 80 m x 80 m. Furthermore, the airport has integrated cargo facilities and hangars for purpose of maintenance. The vertical height between the elevated apron and the runways measures 95 m. The inclination of around 20° is calculated as follows [13]:

$$v_{TO} = 270 \, \frac{km}{h} = 75 \, \frac{m}{s} \tag{1}$$

$$R = 1500 \, m \tag{2}$$

$$a_z = \frac{v_{TO}^2}{R} \tag{3}$$

$$a = \sqrt{g^2 + a_z^2} = \sqrt{9.81^2 + 3.75^2} \approx 10.5 \, \frac{m}{s^2} \tag{4}$$

$$\tan\theta = \frac{v_{TO}^2}{a \cdot R} \tag{5}$$

$$\theta = \tan^{-1}(\frac{\left(75 \, \frac{m}{s}\right)^2}{10.5 \, \frac{m}{s^2} \cdot 1500 \, m}) \approx 20° \tag{6}$$

The airport will be connected to external infrastructure via train rails with a train station and underground roads leading to parking decks integrated underneath the elevated apron. This offers the possibility to create usable space below ground. The cut material of the trenched runway area will be used as noise mitigation.

By using circular runways, take-off and landing windward becomes possible at all times, resulting in fluent traffic without holding in approach nor queueing at the runways. Additionally, cross winds can be avoided and optimal lift during take-off and landing can be achieved. The design furthermore provides a more efficient usage of covered area. For the same performance as a conventional airport only one third of its area is needed [14]. Comparing the size of *RosE's* circular airport (7.07 km²) to the size of Frankfurt Airport (21.6 km²) or New York

John F. Kennedy Airport (19.95 km²), the reduction of used space on ground is significant. The circular airport layout creates an endless runway which is safer in case of emergency. Thus, there is no more decision speed v_1 and emergency landing can be performed with higher landing weights since there are no more limits to take-off and landing distances. Giving the runway a vertical height of about 95 m relative to the apron, around a third of the aircraft's kinetic energy is absorbed during landing and gained during take-off respectively. This is shown in the following calculation, k being the factor of energy saving.

$$\Delta E_{Pot} = k \cdot \Delta E_{Kin} \tag{7}$$

$$m \cdot g \cdot h = k \cdot \frac{1}{2} \cdot m \cdot \Delta v^2 \tag{8}$$

$$\Delta v = 75 \ \frac{m}{s} \tag{9}$$

$$k = \frac{1}{3} \tag{10}$$

$$\Delta h = k \cdot \frac{\Delta v^2}{2 \cdot g} \approx 95 \ m \tag{11}$$

A full model of the airport is shown in the appendix.

5.3. Taxi

In conventional airport and aircraft designs, taxiing consumes an averaged 473 kg of fuel per flight cycle leading to NO_x emissions of 2.5 kg [15] To reduce unnecessary fuel burn, an electric-powered taxi system is used. Conventional aircraft are tugged for push-back but research is carried out at the moment to design a cart capable of carrying the whole aircraft [16]. The designed airport makes use of a battery-powered *Electric Taxi Vehicle* (ETV) for taxiing. A pair of sleighs accelerating on rails carry one aircraft on top of an ETV. Those rails lead from the apron to the runway. The ETV is able to perform fully automated manoeuvres and carries the aircraft from arms to gates. Due to small curve radii in the arms, two sleighs are needed for each aircraft to enable cornering. This requires bearings for the ETV and aerodynamic cowling to reduce drag during acceleration.

At the gates the ETV is being reloaded by induction fields integrated at the parking positions during turn-around. While delivering the aircraft from gates to arms, engines are in idle which causes less emissions and reduces energy consumption. For take-off, the ETV drives onto a sleigh where it is locked.

5.4. Take-Off and Landing

5.4.1. MagLAS System

For take-off and landing, a modified system is used, which is comparable to common magnetic levitation systems used in mass transportation. The aircraft both takes off from the ETV and lands on it. In order to insure this functionality, the ETV is mounted on two magnetic-levitation-based sleighs. This is called *Magnetic Levitation and Acceleration System* (MagLAS). A conventional landing gear is no longer necessary. To provide safe docking, female plugs on the ETV and male plugs on the aircraft are attached. The plugs on the ETV are adjustable in angle to enable landing even in critical situations e.g. in case of sudden crosswinds or any other disturbance influencing the orientation of the aircraft.
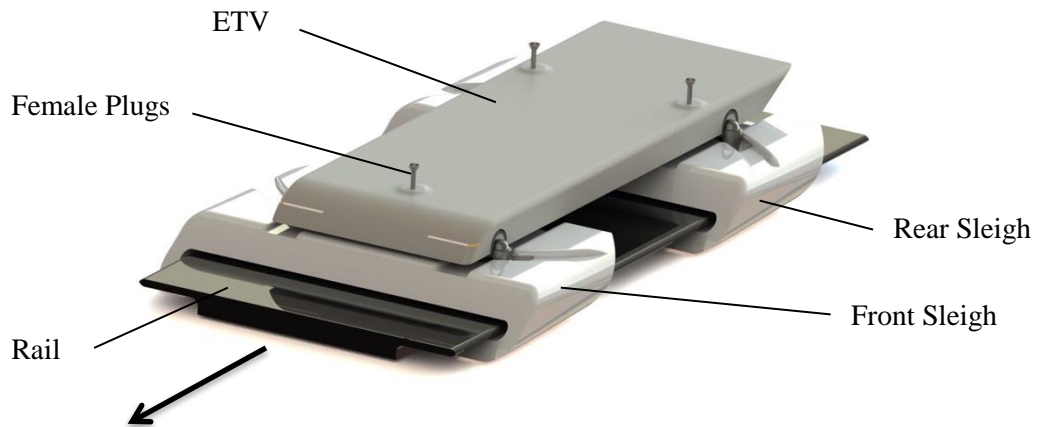
Figure 4: Take-Off and Landing System

5.4.2. Take-Off

Conventional aircraft propulsion systems are designed following requirements from existing take-off procedures. This leads to installed engines being more powerful than needed for the cruise segment. Even climb thrust is only 85 % of the take-off thrust [15]. A circular runway solves that problem as there is no limit to the take-off distance. For conventional aircraft in combination with MagLAS, a noise reduction of 36 % is possible. Furthermore, huge emission drops can be realised as shown in table 2. Flying with engines at a maximum thrust of 85 % of conventional engine's thrust results in weight reductions. The engine dry weight can be lowered, and the amount of mission fuel is diminished.

Type of LTO cycle	CO_2 (kg)	NO_X (kg)	CO (kg)
Conventional LTO cycle	7050	35.57	16.20
LTO cycle with MagLAS (conventional engines)	2961	14.22	6.75

Table 2: Emission Comparison LTO Cycle A330-200 with MagLAS [16] [68]

The acceleration of the sleigh system is initiated on the curved arms and on the runway, which needs to be inclined due to its circular layout. Because the acceleration begins directly at the apron on the arms, the total take-off distance on the circular runway is shorter. Various curve radii and different aircraft weights result in variable centres of gravity. That is why variable force transmissions per track section are necessary. Therefore, the angle of inclination needs to be adjustable, for example by providing a hydraulically adjustable rolling angle via the ETV (see figure 5).
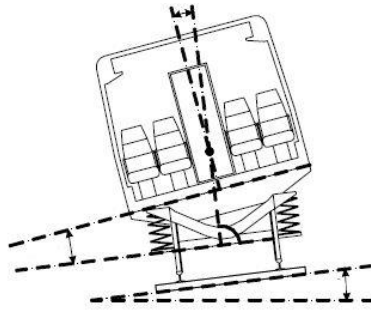
Figure 5: Tilt Technology [17]

5.4.3. Landing

For landing it is essential that the MagLAS is capable of real time synchronisation of the pitching, rolling and yawing angle as well as the aircraft speed. The sleighs adapt to aircraft speed whereas the ETV adjusts its pitching, rolling and yawing angles to the aircraft position. The docking between the aircraft and ETV is done with a male plug extending from the aircraft and a female plug on the ETV.

Due to severe changes on the infrastructure, there must be a step-by-step solution. One possible solution is to land conventional aircraft with landing gear on modified ETVs. The autopilot software would have to be updated so conventional aircraft can land on the vehicles. Later, ETVs and aircraft can be upgraded to be used on solely on MagLAS.

6. Structure

6.1. Fuselage

The fuselage of the *Airbus A330-200* has been adapted for the new aircraft, featuring a diameter of 5.64 m and a length of 57.51 m with four doors on each side [18]. The main advantages of using a conventional fuselage are: no need of new licenses, same ground handling procedures and doors at their defined positions solving earlier discussed challenges of evacuation. The passenger cabin is arranged in the top part of the circular fuselage and offers seating for Business Class, Premium Economy and Economy Class. This configuration offers space for 278 passengers as seen in figure 6.
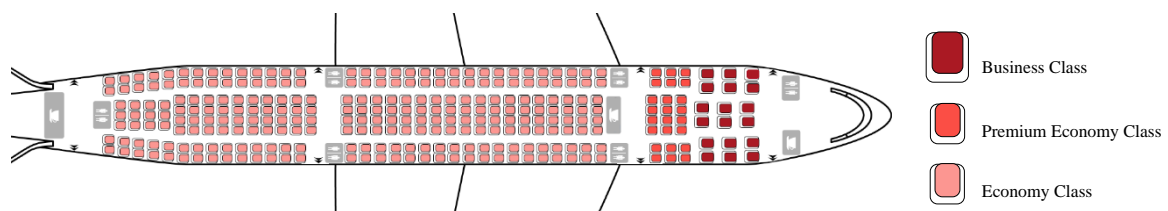
Figure 6: Seating Plan

Positions of galleys, lavatories and closets can be adjusted according to customers' desires. Further advantage of this conventional cabin layout is that there is no need for cabin crew safety training differing from today's standard.

Widespread innovations for materials used in the interior design are introduced. Microlattice, a 93 % nickel and 7 % phosphorous alloy invented by scientists at *UV Irvine, HRL Laboratories* and *Caltech* in 2011 appears to be promising as substitute material for cabin interiors. It is a synthetic, porous metallic material consisting of a periodic array of hollow tubes connected at nodes forming an octahedral unit cell [19]. With a

density of only 0.9 mg/cm³ it is the lightest known structural material. The random cellular architecture of microlattice defines its effective properties like stiffness, strength and good energy absorption [20]. Application in non-structural elements like passenger seats, wall or floor panels provides a significant weight reduction resulting in lower operational costs.

Another promising way of reducing weight within the fuselage construction is to dispense with windows. Common windows consist of three layers of acrylic glass supported by the window frame which requires higher structural stiffness at three points, hence the weight increases to some extent. Furthermore, windows result in higher maintenance effort and costs as they need to be replaced or at least polished every two to three years [21], so, without windows, airlines can save a lot of weight and money. Instead of windows, OLED screens are being used for passenger comfort, only the eight doors keep their windows for emergency reasons. The option to create a 360° view from each seat to display information on the overflown cities or terrain combined with cabin lighting is designed to stimulate the melatonin distribution in passengers' brains. Jet-lag can be reduced which makes flights more comfortable for passengers and crews. Figure 7 gives an example of a possible cabin environment with OLEDs.

Figure 7: Cabin Environment with OLEDs

The skin of the fuselage is made of fibre-reinforced composites as it is already done today. By 2045, developments of lighter materials and technical possibilities to combine materials will have made further progress. Besides, it is expected that aviation will use less riveted joints as they create higher mass, drag and cause high assembling effort. Therefore, research will focus on adhesive joints of carbon-fibre reinforced composites (CFRP) which promise innovative concepts in the future.

Inspection and maintenance is required to ensure safety and reliability of the aircraft. Since 90 % of all inspections are performed visually, an improvement of procedures, efficiency and an extension of inspection intervals is needed. Applying self-healing composite materials to the aircraft structure seems auspicious and offers possibilities to achieve improvements in maintenance time [22]. While composite materials pose a problem for critical structural elements such as wings and fins in maintenance and deployment [23], self-healing composite materials have the ability to counter these problems by independently repairing damages that have occurred during operation. Hence, the lifetime of components will be increased when healing micro cracks before any crack growth or extension leads. Three self-healing concepts are considered to be feasible: capsule based, vascular and intrinsic (figure 8).
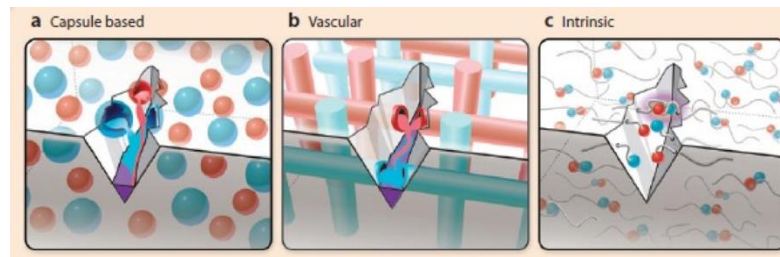
Figure 8: Self-Healing Materials [24]

Capsule-based healing systems utilise healing agents sequestered in discrete capsules. Vascular healing systems deliver the healing agent to a damaged area via an embedded vascular network. In intrinsic healing polymers, a latent material ability is triggered by damage or an external stimulus such as heat, light or pressure [24]. Due to their specific strength and stiffness, combined with significantly reduced density compared to metallic counterparts, fibre reinforced plastics are used in *RosE*'s primary and secondary structure [25]. For self-healing, a series of vascular networks parallel to the fibre direction is applied to repair critical damage such as internal matrix cracking and delamination. Self-healing materials have proven good recovery qualities of mechanical properties when placing self-healing hollow glass fibre plies within a glass-fibre epoxy composite. The self-healing approach offers a significant potential in restoring structural integrity to composite components during service and has prolonging effects on residual strength after damage has occurred [26].

The size of cargo compartments remains constant as for the reference aircraft with a capacity of 60.7 m³ in the forward and 52 m³ in the rear compartment. A total cargo compartment capacity of 112.7 m³ can be utilised for up to 26 LD3 containers or 13 pallets. Additionally, there are 19.7 m³ available for the bulk cargo compartment. Cargo compartments are loaded and unloaded via cargo doors in the lower fuselage section. The ground-handling and turn-around times will be elaborated in chapter nine.

The middle section of the fuselage in between the two cargo compartments is used for the centre wing box. Compared to the A330-200, *RosE*'s centre wing box is widened to approximately 8 m in the aircraft's lateral axis on each side of the fuselage, resulting in a total length of 21.6 m. This leads to the wing being heavier but also increases stability to carry the wing and propulsion system.

6.2. Wing

As mentioned in the previous chapter, the centre wing box is extended on both sides of the fuselage to carry the complex wing structure. The designed configuration combines the advantages of a conventional wing, a blended wing and a box wing.

The transition from wing to the fuselage is shaped as a blended wing, so there is no defined line between these two components. Main advantages of this configuration are the strengthening of the critical connection between wing and fuselage as well as the reduction of the aircraft's ground noise [27]. Another benefit is that electrical fans (e-fans), providing the propulsion, can easily be integrated into the wing. A blended wing profile increases the speed of airflow and guides the air directly to the fans.

The upper surfaces of the e-fans define the geometry of the top wing. The fans are embraced by the top and bottom wing up to 9 m off the fuselage's centreline. The wings then form a box wing with very thin profile shapes. For common box wing designs, the bottom wing is mounted at the front part of the fuselage while the top wing is mounted at the rear part. That is done to maintain constant sweepback, but a second centre wing box would have to be created, in order to gain the needed mechanical stability which ultimately would result in higher weight. In this design, the housings of the e-fans offer sufficient mechanical stability. Combining a box wing with a conventional wing, only the original centre wing box is necessary, and no second centre wing box has to be constructed. With a sweepback between 23° and 28°, for the top as well as the bottom wing, the thin and lightweight profile of the lower wing generates a total span of 52.2 m. This span is about 8 m shorter compared to the *A330-200*, again reducing weight.

The centre wing box itself has two functions. The first one is providing structural connection and supporting the wing. The second one is offering space for the storage of hydrogen tanks and fuel cells. The storage of hydrogen tanks and fuel cells is explained in the following figure.
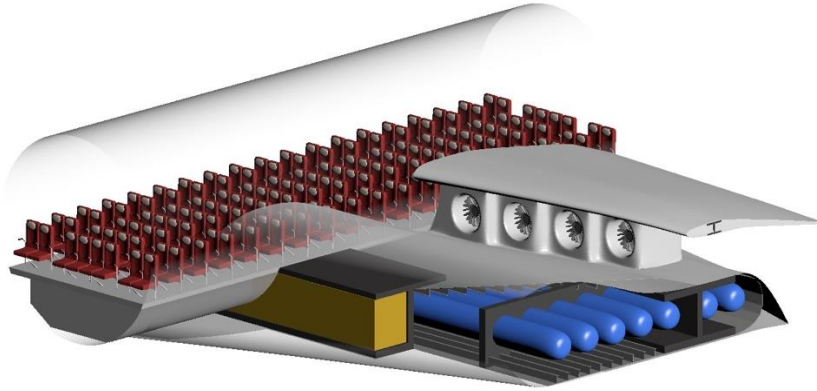
Figure 9: Front Spar and Centre Wing Box with Hydrogen Tanks (blue) and Fuel Cells (yellow)

The centre wing box consists of the main wing spar and the vertical ribs. The larger area of the centre wing box, connected to the wing spar, can carry more force. Regarding figure 9, the maximum height of the wing spar is consequently at the aircraft's centre with a height of about 1.6 m narrowing towards the tips. Conventional aircraft store fuel in the wings, the centre wing box and additional tanks. *RosE*'s centre wing box contains hydrogen tanks and fuel cells that are stored perpendicular to the aircraft's longitudinal axis. Wing ribs are usually designed with holes in it, thus the tanks can be arranged through the ribs and parallel to the spars. In the area where deformations due to aerodynamic loads are neglectable, tanks could be pushed through holes in the ribs without losing stiffness. Using this method makes it possible to store 14 tanks having a diameter of 0.83 m and a length of 10 m in the centre wing box. A total capacity of 115 m³ of LH2 is needed to achieve the same range as the baseline. The 14 tanks result in a total capacity of 250 m³, allowing a return flight to the home base, reducing the turn-around time at destination.

The wing is mostly made of CFRP or lightweight aluminium alloys. To advance its aerodynamic properties, hybrid laminar flow control (HLFC) is used, explained in detail in chapter seven.

6.3. Empennage

The empennage is designed as a V-tail. Compared to conventional empennages, the area is smaller, resulting in reduced drag. To calculate the needed angle and area of the V-tail, following formulas are used [28].

$$\gamma = \arctan\frac{S_V}{S_H} \tag{12}$$

$$S_{V-Tail} = \sqrt{S_H^2 + S_V^2} \tag{13}$$

The area of the *A330-200*'s vertical stabiliser is 47.65 m². The area of the horizontal stabiliser is 31 m². Resulting from formula (1), $\gamma = 41.7°$ and $S_{V-Tail} = 78.2$ m². Compared to the *A330-200* empennage, the area could be reduced to a theoretical minimum of 71.3 %. In practise, this value has to be increased which leads to an empennage area for *RosE* of 80 % of the reference empennage area [28]. A conventional tail has three interfaces, one for the vertical and two for the horizontal stabilizers. A V-tail needs only two interfaces, one on each side of the fuselage, resulting in less construction effort and reducing the total mass of the rear section.

Although the complexity of the V-tail adjustment is its main disadvantage, it can be expected that there will be high-precision sensors capable of controlling the advantageous empennage by 2045.

7. Aerodynamics

7.1. Morphing Wing

By 2045, it will be possible to reduce mechanic elements in wings such as flaps or control surfaces. Usually, a wing is designed for highest efficiency in cruise. For take-off and landing, flaps on the leading and trailing edge are extracted to increase lift and to adjust the lift-to-drag ratio. Depending on the manoeuvre, the wing surface and the wing vault are changed. To reduce the number of components and to decrease weight, flights will be performed using morphing wings that can be realised through different methods. Shape memory alloys, mechanic actuators or piezo-electric materials can be taken into consideration. Advantages of using morphing wings are reduction of maintenance effort, noise reduction, mass minimisation and finally a reduction of the energy consumption. Research on this topic has been conducted by team member A. Rahn [29]. *RosE* only has rudders on the empennage. For certification, stall capability has to be proven.

7.2. Hybrid Laminar Flow Control

To improve aerodynamics, to reduce overall aircraft drag and to achieve an eco-friendly aircraft, a so-called *Hybrid Laminar Flow Control* (HLFC) is used [30]. This active drag reduction system controls airflow over wetted surfaces during cruise. Laminar flow systems aim at delaying the transition from laminar to turbulent airflow over wing or empennage aerofoils. The relevant transition mechanisms on transonic swept wings are defined by *Tollmien-Schlichting Instability* (TSI), *Attachment Line Transition* (ALT) and *Crossflow Instability* (CFI). The application of suction systems over the first 10-20 % of the chord controls the CFI and ALT of swept wings [31]. Wing shaping and adjusting aerofoil geometry for favourable pressure gradients suppress TSI and therefore transition. HLFC is proven to be the best concept for drag reduction besides *Natural Laminar Flow* (NLF) [32]. HLFC integrates NLF (wing shape and aerofoil geometry) and active laminar flow control, for example by a mechanical suction system. The suction system implemented in *RosE* consists of a simplified one presented by the *European ALTTA* and a tailored hybrid outer skin presented by Horn [33] [34]. Removing air from the boundary layer through a perforated skin with an existing pressure difference between surface and plenum chamber, the velocity profile is modified, and the boundary layer is reduced which positively influences the associated Reynolds number. The necessary pressure difference between the outside flow and the plenum chamber is achieved using a compressor. The hybrid skin controls the pressure difference in span- and chord-wise direction. The tailored outer skin consists of a micro-perforated metal sheet with an underlying multilayer metal mesh.

The HLFC skin surface is a primary structural element which is rated a class one part for safety and certification issues [35]. Prevention of failure and of separation of the panel from the wing structure, such as satisfactory strength, stiffness and fatigue properties, are required. Due to micro perforations, the surface cannot be painted which causes problems regarding corrosion resistance. To avoid this, the best choice for the base material is thought to be titanium as it is a light material offering advantageous corrosion characteristics.

Favourable wing parameters for HLFC are a wing sweep of 23°-28° and Mach numbers of 0.805-0.836 [36]. The reduced Mach number of 0.75 used for *RosE* has only minor influence on the effect of the HLFC which therefore is neglected. An optimally profiled and HLFC-equipped wing could permit laminar flow for up to 50 % of the chord length. This results in a local drag reduction of 29 %, which leads to an overall drag reduction of 6 % for the aircraft [30].

7.3. Sharkskin

The application of HLFC systems, as described in the prior chapter, was tested successfully. However, due to turbulences still present at aerofoils, a certain amount of skin friction remains. The 'sharkskin effect' is based on the dermal surface morphology of sharks and implemented as an innovative technology to improve aerodynamic

performance [37]. Application of riblet coatings reduces the displacement thickness of the boundary layer. This virtually increases the aerofoil camber and produces an aerofoil with higher lift [38]. The microstructure of the riblets changes the distribution of the flow field and reduces wall shear stress and skin friction drag. The geometry of the riblet coating must be suitable to the Reynolds number of the wing surface and aircraft body [39]. Depending on the geometry of the riblets, a skin fraction drag reduction up to 8 % is achievable [40]. The following surfaces of *RosE* are covered with small riblets aligned in the local flow direction: the upper half of fuselage surface, the empennage surfaces and the upper half of the wing surfaces beyond leading edge micro-perforations. The skin friction amounts to about 50 % of the total drag, leading to a 4 % drag reduction in total [38]. The technology application used for *RosE* was developed by *IFAM Fraunhofer* as alternative solution to bonded riblet foils (e.g. *3M*). The advantage of the *IFAM* technology is that three-dimensional surfaces can be painted with a functional riblet surface without any additional process steps. The coating is a single step application, embossing and partial curing by ultraviolet light [39]. Removing the riblet coating in case of maintenance and structural repairs can be avoided by application of self-healing composite materials. These prevent failure and extend durability of critical structures, eliminating the sharkskin's major disadvantage.

8. Propulsion System

8.1. General

Main goal of *RosE* is, in accordance with *NASA*s ARMD, the reduction of energy consumption mentioned in chapter two. As outlined in *ARMD Thrust 4*, the introduction of alternative propulsive systems such as electric/hybrid-electric propulsion from 2035 on will be a major step towards low-carbon propulsion [41] and has therefore been the main reason for focusing on a fully electric propulsion system. This decision was reinforced by *NASA*s prediction that ground-breaking changes will not solely be achieved by evolutionary technology improvements and the outlook on radically increased environmental benefits for non-petroleum-based concepts [42].

While hybrid-electric aircraft have shown the potential to reduce fuel burn by up to 54 % [43], a fully electric propulsion system additionally offers a higher efficiency and zero in-flight NO_x and CO_2 emission, making it the most promising candidate technology to date. Amongst the electrical machines used in a fully electric concept, one relatively young technology stands out. In contrast to the insufficient power densities of conventional motors in the range of 1 kW/kg, which is too heavy for most mobile applications [44], high temperature superconducting (HTS) machines offer great advantages. Predicted high power densities of up to 25 kW/kg and electrical efficiencies of 95-99.5 % [45] by far surpass conventional gas turbines, making HTS the ideal technology for future applications and are therefore the technology chosen for *RosE* [46]. Research supported by *NASA* and conducted by Masson and Luongo paves the way for further investigation by showing that the use of superconducting motors is, in fact, possible in aircraft [44].

To power the electric motors, an energy system with short reaction time capable of delivering an adequate amount of electricity at any given point in flight must be implemented. Possible solutions range from the use of conventional gas turbines fed by kerosene, bio- or alternative fuel, to storing the needed amount of electrical energy in batteries, to producing electricity during flight via fuel cells fed with liquid hydrogen (LH2).

The use of kerosene or biofuels to generate electricity with a gas turbine has been subject of investigation in order to use it in the process of changing to sustainable propulsion. However, they are not an ideal long-term replacement for fossil fuels [47] and offer only marginally better exhaust values. In conclusion, the use of a gas turbine would undermine the goal of cutting NO_x emissions and has therefore been disregarded.

Batteries lack the required energy densities [48] and although this is likely to change until the potential EIS of *RosE*, they have been dismissed, too. This decision was based firstly on the fact that batteries do not lose weight while discharging, leading to reduced flight range, and secondly on findings of Tan et. al. concluding that batteries do not show the potential for usage in large civil aircraft in 2045 [49].

For these reasons, the *RosE* concept features an energy system that uses fuel cells fed with LH2. Composition, advantages, disadvantages, feasibility and performance characteristics of both the propulsion and energy system will be discussed in the following.

8.2. HTS Propulsion System

8.2.1. System Description

An HTS propulsion system for the setup introduced in 8.1 consists of multiple supercooled rotary machines, two or more cryocoolers, a controlling entity, a distribution system for electricity and connection between motors and cryocoolers. Cryocoolers may be unnecessary when using LH2 as cryogen. This possibility will be discussed in 8.2.3.

8.2.2. HTS Motors
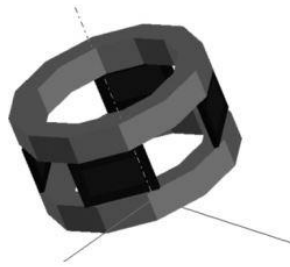
Figure 10: Assembly of the Inductor Composed of Pancake Coils and Bulk Plates [44]

For most aircraft drive systems, rotary machines with HTS stator windings and permanent magnets or wound and trapped-field rotors are preferred. The stator is generally constructed by winding HTS tape flat on spools of the same width, over each of the poles, which are quite large. In figure 10 such windings that are referred to as pancake coils are shown [50] [44]. The possibility to integrate the motor into the hub of the propeller results in a very compact design (figure 11).

Concerning the propulsive efficiency, it is of utmost importance to drive the propeller at an advance ratio, so it is always operating at the maximum propulsive efficiency point. This necessitates the use of a maximum propulsive efficiency point tracking (MPEPT) outer loop [50]. Compared to traditional electric machines, HTS motors not only have a tremendously better specific power ratio and higher efficiency but also outperform them in terms of values of inductive parameters, noise level and stability of on-load regime [51].
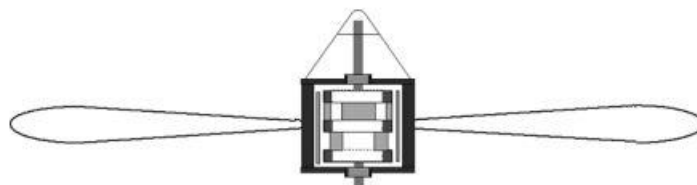
Figure 11: Superconducting Motor Embedded into the Propeller [44]

In terms of the adequate number of HTS motors, literature suggests using multiple smaller engines rather than a few large engines. Numbers of eight to 16 individual motors have been suggested [52]. The use of multiple motors arranged next to each other on the upper side of each wing yields a large total area and a high effective bypass ratio, enables the use of a Hybrid Laminar Flow Control as discussed in chapter seven as well as the possibility to manipulate the aircraft's orientation around its vertical axis, the possibility to adapt each propeller's rotational speed to its respective position on the aircraft and a very high grade of redundancy [53]. Since a dramatic yawing moment is not to be expected in case of engine failure, an analysis of a one-engine failure case was deemed unnecessary.

Under certain conditions, it could be possible to use the motors as generators to regain electrical energy during descent.

8.2.3. Cryocooling

While initially the positive effects of superconducting electrical machines have been limited to temperatures of 20-30 K, more recent findings suggest that operating temperatures of 50-77 K will be achievable in future generations of HTS machines. This is assumed to be the range of operation temperature for *RosE* [52] [53].

Currently, there are no low weight cryocoolers available that can produce the needed power since most work in this area is done for on-satellite use with low power demand [54]. Refrigeration powers of 1-10 kW at 50-65 K with a Carnot efficiency of 30 % are required. Current specific weights range from 10-30 kg/kW with efficiencies of about 20 %. This is faced by an on-aircraft demand for a specific weight of 3 kg/kW [55].

It has generally been accepted that reverse-Brayton cycle cryocoolers will be most suitable for high power aircraft applications due to their scalability and reliability. The most sensible concept for cryocooling components aboard aircraft is a centralised system in which large cryocoolers provide a circuit of fully cooled cryogen or an open circuit [52].

However, since *RosE* features LH2 power supply in which hydrogen is stored at around 20 K, the use of cryocoolers is superfluous. An open circuit of expendable cryogen, such as LH2, driven by pumps and cooling the components directly is utilised since this promises the lowest specific mass. This might change if targets of 3 kg/kW cryocoolers become achievable [52] [54]. For the sake of reducing weight and since EIS lies far in the future, it has been assumed that dedicated cryocoolers will not be necessary.

8.3. Electrical System

8.3.1. Introduction

The concept for *RosE*'s electrical system features a unique way of storing chemical energy and transforming it to electrical energy. This, in combination with an HTS propulsion system, has never been focus of scientific work and is therefore highly theoretical, although it is thought to have the potential to enable the clean and very efficient air traffic sought after.

As source of energy, liquid hydrogen is used, which is stored in specially insulated cryogenic tanks and then transformed to electricity through highly efficient fuel cells with high specific power.

LH2 has been selected because of its high mass reduction factor compared to kerosene, its superior specific energy of 119.9 MJ/kg, the possibility of it being used as cooling means for the HTS machines instead of dedicated cryocoolers, its eco-friendly exhaust emissions (water) and the fact that it can be produced sustainably via electrolysis, solar conversion or biomass gasification. The separation of power and thrust production, as well as the omission of Auxiliary Power Unit (APU) and Ram Air Turbine (RAT), together with the beforehand mentioned advantages make the combination of cryogenic hydrogen storage and a fuel cell-supplied propulsion system superior to the conventional system [56]. An existing several hundred kilometres of hydrogen pipelines show that the extensive distribution of LH2 is both possible and safe [57].

8.3.2. LH2 Storage

Amongst the several possible ways of storing hydrogen, only liquid hydrogen appears to be feasible in aviation [58], but to keep the hydrogen in its liquid state at 20 K, insulated tanks are necessary.

Tanks can have cylindrical, elliptical, complex or obround designs. For this system, elliptical tanks of 10 m and a capacity of 18.17 m^3 each have been chosen. These dimensions fit best for the integration in the centre wing box and allow high payload-mass fractions. For a range of approximately 10,000 km, at least seven such tanks will be necessary. A higher number of tanks seems beneficial since refuelling time can be reduced due to the possibility of multiple tanks being refuelled simultaneously. A study conducted by *NASA* identified the aluminium alloy 2219 to be best suited to the stresses from the supercooled hydrogen [59].

The choice of the insulation material is an important factor for the performance of the storage system. Light-weight insulation is of importance, as Direct Operating Costs (DOC) are linked to aircraft weight and fuel consumption. Also, strict safety requirements must be fulfilled and high temperature differences between inner and outer tank wall have to be endured. Since literature does not suggest any materials for insulation additional research needs to be done.

Cooling of the tanks by an external power source is necessary for ground handling times. During flight this might also be required but due to the very low boil-off rate of 3 % per day, it seems unlikely to be needed in future applications.

Because of those boil-off effects, the pressure inside the tanks increases. This entails the need for a venting mechanism, to maintain or decrease the pressure level inside the tank and therefore ensure the security and integrity of the tank system. To keep the danger of combustion as low as possible, the minimum pressure of the tank should always be slightly above the maximum atmospheric pressure. Hereby, it can be guaranteed that no oxygen enters the tank, which would lead to an explosive mix of gases.

8.3.3. Proton Exchange Membrane Fuel Cell

Proton Exchange Membrane Fuel Cells (PEMFC) have been chosen for having the best efficiency amongst fuel cells. Although the current efficiency of these types of cells is up to 70 %, it can be assumed that efficiencies of 85 % can be reached. Also, since they have already been used in the automotive sector, their usability and reliability has been proven. PEMFC have a specific power of up to 2 kW/kg and produce heat that might need to be countered by a cooling system but could also be used for de-icing and heating of the wing area.

Since most of the so far conducted scientific research on HTS propulsion systems have made use of an AC architecture, heavy inverters had to be implemented, lowering the feasibility of those systems. Since fuel cells produce DC, *RosE* can utilise advantages like minimized electrical losses, superior flexibility and robustness of such an architecture without the need for power electronics with enormous weight penalties [54]. Voltage requirements that have been found to be around +/- 3 kV can be met by connecting multiple individual cells with each other [45] [60] [53]. The hereby formed stacks have an increased voltage output.

Since the production of electricity generates the by-product H_2O, a way to deal with the forming water needs to be developed. One possibility is to simply release the liquid into the atmosphere. Although the effects of H_2O vapour on the environment are somewhat less dramatic than those of NO_x or CO_2, negative impacts are undeniable [61]. To better comprehend these effects, further research is necessary.

A second possibility to deal with unwanted water is to produce hydrogen which can be fed back into the tanks. The needed electricity for this process could be gained from solar panels mounted on the wings and fuselage. Since the maximum fuel cell power output must fit the maximum load occurring during the climb segment, and because the fuel cells work most efficiently at 90 % of maximum capacity, a part of the fuel cells will be inoperative in normal cruise condition. Those usually inoperative fuel cells could also be used to work as 'chargers', producing hydrogen from the by-product H_2O and the electricity gained from solar panels.

8.4. Performance Evaluation

8.4.1. Introduction

As mentioned in the beginning of this chapter, goals of this concept study are a reduction of energy consumption of 60-80 %, reduction of LTO and cruise NO_x emission by at least 80 % and the noise by 42-52 dB compared to a baseline *A330-200*. To be able to compare the performance data, an approximate calculation of both aircraft's performance needed to be established. A stripped-down description of the calculation and the findings of the calculation will be presented in the following. Detailed calculations can be found in the appendix.

A typical airliner mission profile as seen in figure 12 has been used for reference.

Distance [km]	–	–	30	8	270	8	8460	130	10	50	10	–
Time [min]	10	2	4	1	20	1	624	10	1	5	8	5
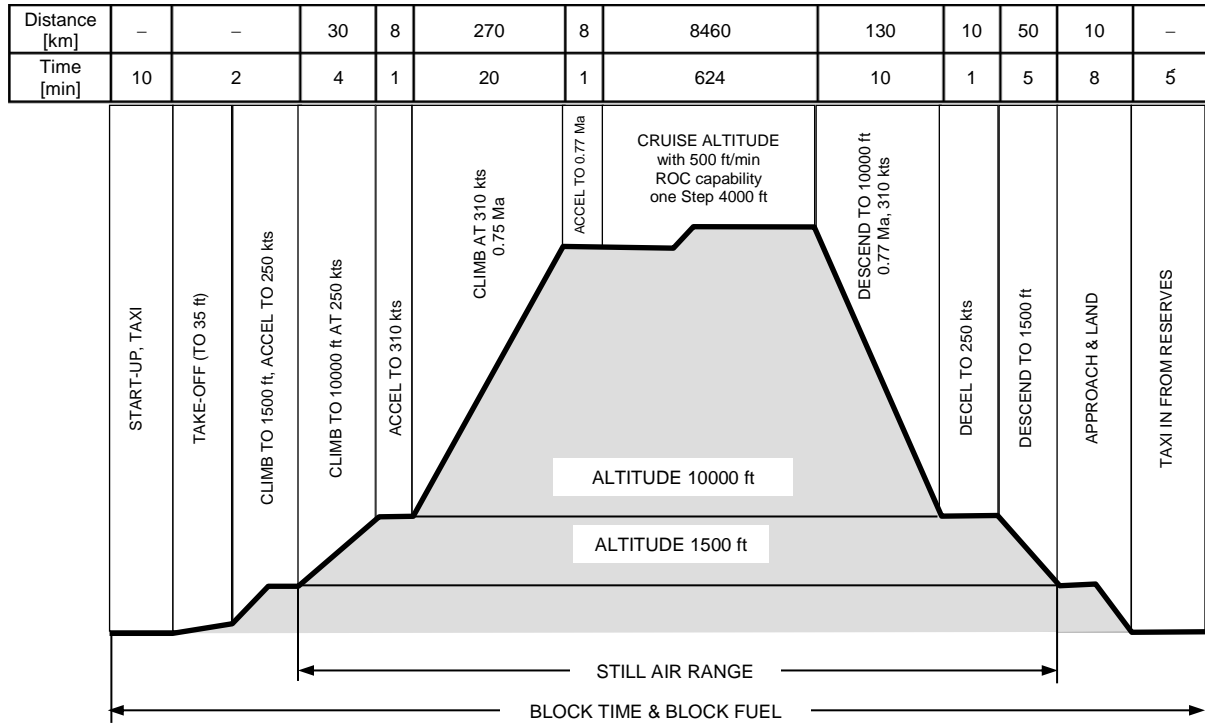
Figure 12: A Typical Mission Profile of an Airliner from Take-Off to Landing [62]

8.4.2. Baseline Aircraft Performance

To be able to calculate important and reliable benchmark data for aircraft, credible base-data is necessary. For this calculation, aircraft dimensions from *Airbus*' documentation of the *A330*-family [63] and for engine specification an official *EASA* data sheet [64] have been used. Temperature and density calculations are based on the International Standard Atmosphere.

Firstly, the calculation of the drag coefficient c_D was done:

$$c_D = c_{D0} + c_{Wi}(c_L) + c_{WW}(c_A) \tag{14}$$

where c_{D0} is the parasite drag coefficient, c_{Wi} is the induced drag coefficient and c_{WW} is the wave drag coefficient which has been neglected due to relatively low values for Ma < 0.85.

The vertical equilibrium of forces in stationary cruise conditions dictates:

$$L = m \cdot g = \frac{\rho}{2} \cdot v_{A330}{}^2 \cdot c_L \cdot S_W \tag{15}$$

where L is the lift in N acting on the aircraft, m is the mass in kg of the aircraft, g is the standard gravity of 9.81 m/s², ρ is the air density at flight altitude in kg/m³, v is the cruise velocity in m/s and S_W is the surface area of the wings in m². From this, c_L can be calculated.

From the mass of fuel inside the tank after take-off and climb, $m_{F,cruise}$, and the specific energy of kerosene, $e_{Kerosene}$, the energy stored in the tank for cruise can be calculated:

$$E_{Tank,cruise} = m_{F,cruise} \cdot e_{Kerosene} \tag{16}$$

removing f_L, an approximated 10 % from $E_{Tank,cruise}$ for powering of electronics, pressurized cabin, avionics, etc., and involving the efficiency of a gas turbine gives the energy remaining for propulsion:

17

$$E_{Prop,A330} = \eta_{Turbine} \cdot (1 - f_L) \cdot E_{Tank,cruise} \tag{17}$$

With the horizontal equilibrium of forces for stationary flight,

$$T = D = \frac{\rho}{2} \cdot v_{A330}{}^2 \cdot c_D \cdot S_W \tag{18}$$

the required thrust T_{req} can be calculated. The factor f_T is calculated:

$$f_T = \frac{T_{TO}}{T_{req,A330}} \tag{19}$$

Now, the required propulsive power, P_{req} at cruise velocity v,

$$P_{req} = T_{req} \cdot v_{A330} \tag{20}$$

is found. The flight time at required propulsive power for the remaining energy can be calculated:

$$t_{Cruise} = \frac{E_{Prop,A330}}{P_{req}} \tag{21}$$

With help of the cruise velocity, a range can be determined:

$$s_{Cruise} = t_{Cruise} \cdot v_{A330} \tag{22}$$

For take-off, consisting of a ground run and a climb to 1500 ft at 250 kts, a simple physical calculation has been performed including the take-off mass m_{TO}, take-off thrust T_{TO}, the efficiency of a gas turbine $\eta_{Turbine}$, the estimated maximum lift coefficient $c_{L,max}$, the resulting take-off speed v_{TO}, the time at take-off thrust t_{TO}, the height h_E and the velocity v_E at segment end:

$$E_{req,TO} = \frac{1}{\eta_{Turbine}} \cdot \frac{1}{2} \cdot m \cdot v_E^2 + m \cdot 9,81 \frac{m}{s^2} \cdot h_E + T_{TO} \cdot v_E \cdot t_{TO} \tag{23}$$

for the climb segment to 3500 ft at 310 kts, this simplifies to

$$E_{req,Climb} = \frac{1}{\eta_{Turbine}} \cdot \frac{1}{2} \cdot m \cdot v_E^2 + m \cdot 9,81 \frac{m}{s^2} \cdot h_E \tag{24}$$

The total energy consumed for take-off, climb and cruise is composed of the energies calculated above:

$$E_{req,Total} = E_{Tank,cruise} + E_{req,TO} + E_{req,Climb} \tag{25}$$

Based on these formulae, the following values have been calculated:

	value	
c_D	0.031	
$m_{F,Cruise}$	65,000	kg
s_{Cruise}	10,540	km
$E_{Tank,Cruise}$	2,697	GJ
$E_{req,TO}$	7	GJ
$E_{req,Climb}$	31	GJ
$E_{req,total}$	**2,735**	**GJ**

Table 3: Performance Data of A330-243

8.4.3. *RosE* Concept Performance

Based on the assumption that the new aircraft should preferably have similar dimensions as the baseline to insure the compatibility with current airport layouts, several variables were already set. Also, since the challenge requirements dictate the new design to have equal or better mission parameters, cruise velocity, range and payload are fixed.

Going from this, it was necessary to add a number of parameters. Since designing aircraft in detail is an extremely elaborate and time-consuming process, many of these parameters have been estimated using statistics to ensure a simplified and comparatively fast but not very exact calculation. The following results represent a rough estimate that enables comparison, but additional calculations, simulations and test are needed for a more realistic result.

However, starting with mentioned dimensions, the calculation of c_D, c_L and L/D_{opt} have been possible. Since *RosE* features a box wing configuration, additional calculation of the reduction of induced drag $c_{D,i}$ had to be done. Schiktanz et. al. propose the following formula [65]:

$$\frac{D_{i,box}}{D_{i,ref}} = \frac{0.44 + 0.9594 \cdot \frac{h}{b}}{0.44 + 2.219 \cdot \frac{h}{b}} \tag{26}$$

Where h/b is the height-to-span ratio of the configuration and D is the Drag in N. In order to calculate the induced drag coefficient $c_{D,i,box}$, the equation has to be changed to

$$c_{D,i,box} = c_{Diref} \cdot \frac{S_{Wref}}{S_{WBox}} \cdot \frac{0.44 + 0.9594 \cdot \frac{h}{b}}{0.44 + 2.219 \cdot \frac{h}{b}} \tag{27}$$

Analogous to the *A330-200*, the required thrust and the required propulsive power at cruise can be calculated. From the required propulsive power at cruise and the required flight time calculated from the new, lower flight velocity and the fixed range, incorporating the efficiencies of the motors η_{HTS}, of the fuel cells η_{FC} and the propeller η_{Prop}, and the factor f_L that has been introduced earlier, the required energy stored in the tank can be calculated:

$$E_{Tank,Cruise} = \frac{1}{\eta_{HTS} \cdot \eta_{FC} \cdot \eta_{Prop} \cdot (1 - f_L)} P_{req} \cdot t_{Cruise} \tag{28}$$

19

For the take-off and climb segment, the same approach as with the *A330-200* has been applied but due to the reduced drag, a reduction of energy that is proportional to the reduction of the drag, ΔE_{Drag}, has been subtracted. With equation (18), the required thrust for *RosE* is calculated. T_{TO}, which is the fundament for the design of motor and fuel cell mass, is calculated bearing the reduction to 85 % of take-off thrust mentioned in chapter 5.4.2 as following:

$$T_{TO,Rose} = 0.85 \cdot f_T \cdot T_{req,Rose} \tag{29}$$

The total required energy is given as follows:

$$E_{req,Total} = E_{Tank,cruise} + E_{req,TO} + E_{req,Climb} - \Delta E_{Drag} \tag{30}$$

Based on these formulae, the following values have been calculated:

	value		compared to baseline	
c_D	0.024		-22.6	%
$m_{F,Cruise}$	7,527	kg	-88,4	%
s_{Cruise}	10,540	km	100	%
$E_{Tank,Cruise}$	856	GJ	-68,3	%
$E_{req,TO}$	2.36	GJ	-64,7	%
$E_{req,Climb}$	23	GJ	-24,8	%
ΔE_{Drag}	-6.00	GJ	-	%
$E_{req,total}$	**875**	**GJ**	**-68**	**%**

Table 4: Performance Data of RosE

To achieve the energy reduction, two trade-offs had to be made. Firstly, the cruising altitude had to be increased to 45,000 ft. This reduces drag and is made possible by the engine modifications. Secondly, the cruise speed was decreased to Ma 0.75 resulting in a 3.3 % energy reduction compared to the baseline aircraft while at the same time not increasing flight time drastically.

9. Concept of Operation

9.1. Ground Handling

The turn-around time for an *A330-200* with full service including passenger handling, boarding, cargo, refuelling, catering, positioning and removal of ground vehicles (figure 13) is 51 minutes. The passenger handling is calculated with 25 passengers per minute and door for deboarding, while the boarding speed is approximately 15 passengers per minute and door. *RosE*'s cabin offers space for 278 passengers. Assuming that *RosE* will use two boarding bridges, as the reference aircraft, time for passengers to leave and enter the aircraft will take less than 15 minutes. Time for unloading and loading the cargo compartments is equivalent to the *A330-200* because the cargo compartments have the same size and the cargo doors have the same position. Usually the cargo compartments are filled with LD3 containers and pallets. Unloading and loading these two as well as the bulk compartment is done simultaneously with an estimated time of 30 minutes for this procedure.
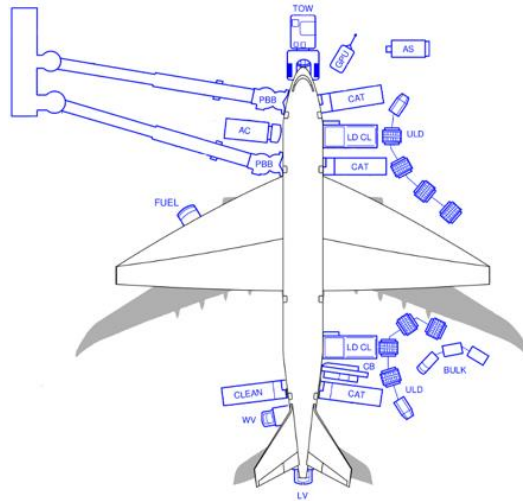
Figure 13: Ground Handling Compared to A330-200 (grey)

Boarding, cargo, catering, positioning and removal of ground vehicles of *RosE* takes the same time as for the A330-200. Most time on ground is needed for refuelling. The time needed to refuel a conventional aircraft with jet fuel is approximately 45 minutes, including positioning the vehicle. Refuelling *RosE* with LH2 takes up to 13 hours calculated with the current flow rates of 1.412 m³/h [66], which is much longer than for conventional aircraft. This is a disadvantage compared to the *A330-200*. However, the principal aim is to ensure eco-friendly air traffic. In this case, this disadvantage can be accepted due to the positive environmental impact [18].

9.2. Safety

9.2.1. Emergency Landing

While conventional aircraft use their landing gear to touch down on the ground during an emergency landing, *RosE* is not equipped with such as it is not designed for landing on conventional runways. Figure 4 in chapter five shows how the landing system is constructed for docking via its male plugs at the destined female plugs on the ETV. As these obviously cannot be used for safe direct contact after touch down, *RosE* uses extendable skits which are – when in retracted position – just a part of the fuselage. However, when emergency landing becomes necessary this system can easily be lowered even in the severe case of electrical dysfunction as it is backed-up mechanically.

Figure 14: Emergency Landing Skids

It is thought that there is no need to design the system for more than one use during the aircrafts lifetime since generally emergency landings damage structural components too much as that such aircraft could be put into commission again. Therefore, the skid-system is designed compromising and balancing adequate structural stability for a one-time use, keeping structural weight as low as possible (figure 14).

9.2.2. Evacuation

The *A330-200* has eight doors that can be used in case of an emergency. There are six passenger/crew doors of which four are in front of the wings and two in the back of the aircraft. Those doors each have one dual lane escape slide that is installed in containers underneath. The remaining two emergency doors right behind the wing have a single lane escape slide (figure 15) [18]. Since the original *A330-200* fuselage was taken for *RosE*, the door positions and the number of passengers remain constant. As safety always is highest priority in aviation, evacuation during an emergency is unexceptionally provided. The emergency procedure according to *EASA* will be the same for *RosE*. It has to be demonstrated that the aircraft can be evacuated in 90 seconds or less with only half of the doors used [67].
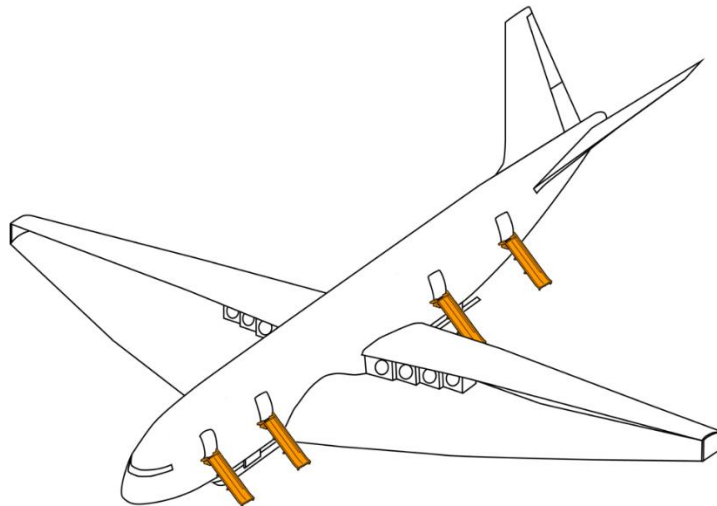
Figure 15: Emergency Configuration

10. Comparison

The aspects shown in the previous chapters lead to considerable mass reductions, which are listed in the following table. In summary, this results in a mass reduction of 32.1 % of the maximum take-off weight of the reference aircraft.

Kind of mass	A330-200 (kg)	RosE (kg)	Reasons; factor
Structural mass	**87,058**	**70,636**	
Wing	37,091	44,509	extended wing box & structure; multiplied by 1.2
Fuselage	32,841	19,705	fuselage is consistent, CFRP, windowless, less rivet joints
Empennage	3,435	2,748	V-tail, no vertical tail weight reduction by 20 %
Landing gear	9,902	2,674	no landing gear; see calculated value (0.27)

Engine installation	3,788	0	neglectable
Emergency landing skids	0	1,000	skids as part of fuselage
Propulsion	**15,217**	**18,112**	
Engines	11,596	882	see calculated value
Thrust reversal	2,114	0	done by e-fans
Subsystem	642	963	see extra apportionment
Fuel system	865	1,297	multiplied by 1.5
Fuel cell	0	11,026	see calculated value
Tanks	0	3,944	see calculated value
Equipment	**22,291**	**18,325**	
ECS	2,395	3,592	weight of compressors relative to pneumatics; multiplied by 1.5
Hydraulic & pneumatic system	1,974	0	inexistent
Electrics	2,048	4,095	multiplied by 2
APU	783	0	inexistent
Flight control	2,855	1,999	fly-by-light
Avionics	1,657	1,657	multiplied by 1
Interior	10,580	6,982	microlattice; multiplied by 0.66
Operational items	**4,329**	**4,329**	
Crew	1,040	1,040	multiplied by 1
Consumable	2,783	2,783	multiplied by 1
Safety equipment	506	506	multiplied by 1
Operating Empty Weight (OEW)	**128,895**	**111,402**	
Payload	**39,105**	**39,105**	
Zero Fuel Weight (ZFW)	**168,000**	**150,507**	
Fuel at maximum Payload	**65,000**	**7,649**	see calculated value
Maximum Take-Off Weight (MTOW)	**233,000**	**158,156**	

Table 5: Comparison of Masses [70]

11. Conclusion

The report at hand, presented by a team of *TU Dresden*, is an attempt at designing an aircraft that combines previously unseen efficiency with a radical reduction of consumed energy and a total cut of CO_2 and NO_x emission. Starting with thorough and extensive research of scientific literature, followed by discussion and several stages of calculation, evaluation and recalculation, the most promising technologies and their subsequent implementation into the concept have been identified. The beforehand stated goals were achieved by a combination of changes to the airport layout, the airport's infrastructure and radical changes to the aircraft itself. Some of those changes have already been relatively well investigated, are in an advanced stadium of research and could therefore be described in great detail. Others have only recently emerged and are currently under-developed but show great potential and have therefore been subjected to a certain extent of speculation.

Aiming at a maximisation of operability, effectivity and used area while simultaneously reducing noise pollution, a ring-shaped airport was found to be a vital part of any attempt to create an eco-friendly air transport system. Such a design not only makes the best use of building ground by reducing the total airport area while maximising the useable area. Furthermore, fluent traffic can be guaranteed due to a virtually endless runway that enables continuous windward take-off and landing. Extended runway length also increases safety while the difference in height between runway and apron reduces energy used for taxiing to the runway and opens the possibility to recuperate energy while running down kinetic energy from landing. A tremendous reduction of the aircraft's mission energy consumption has been achieved by executing taxiing and the take-off segment's ground run by means of the MagLAS moving system, decoupling both procedures from the aircraft's energy household. A novel Electric Taxi Vehicle enables both take-off and landing from such a magnetic levitation system by automatically adjusting its alignment relative to the aircraft.

The original fuselage of the *A330-200* was adapted because of existing licensing, assembly lines and no further needed development efforts. Removal of almost all windows increased structural stability and, like the introduction of microlattice and the use of fibre-reinforced composites, also reduced weight.

Striving to minimise losses due to friction drag, the use of sharkskin in combination with self-healing materials has been implemented on certain parts of the aircraft, reducing drag by 4 %. It was possible to reduce drag by another 6 % by implementing Hybrid Laminar Flow Control into the wings.

The wings have been designed as a hybrid of conventional wing, blended wing and box wing, combining each design's advantages like enlarged storage space, reduction of ground noise and reduced induced drag. A V-tail empennage reduces area and drag of the empennage.

Revolutionary changes have also been made to the energy and propulsion system. The use of highly efficient and powerful High Temperature Superconducting machines is a step towards fully electric propulsion which has been identified as the only way towards low-carbon propulsion and eco-friendly air traffic. The choice of liquid hydrogen as energy source introduces a number of advantages like a far superior energy density compared to kerosene, resulting in reduced weight, the possibility to produce LH2 through sustainable and eco-friendly ways and the possibility to omit heavy cryocoolers by cooling the HTS motors directly with fuel stored at 20 K. To connect energy storage and propulsion, energy transformation through fuel cells has been chosen. This keeps overall efficiency on a level that far surpasses those of thermodynamic systems also producing direct current, so no heavy inverters or power electronics are needed to reap the benefits of a DC architecture. Finally, the use of fuel cells reduces the emissions of *RosE* to only one, useful by-product: water.

A complete and immediate introduction of mentioned technologies is highly unlikely and was never the aim of this concept. Although the outlook brought on by this paper are tremendous, airports, operators and passengers are not ready yet to adapt to such widespread changes. However, a step-by-step introduction is possible and is probably the best way towards the air transport of the future. The first step could be implementing the MagLAS to current airports. Aircraft could easily be retrofitted to be able to land both on our sleighs and on conventional runways.

As the work on this paper draws to an end it also becomes obvious that for a successful implementation to aircraft many things still need to be done. The predicted refuelling time amounts to 13 hours, which means that a procedure allowing higher mass flow rates must be developed. Although some papers expect the HTS motors to reach a specific power of up to 40 kW/kg, even less powerful systems are yet to take flight. Another factor to be considered is the reception by passengers but since the only changes clearly visible to passengers, the MagLAS

take-off and landing system and the continuous OLEDs, are fairly well known to the public, the adaptation to these innovations is expected to occur unproblematically.

In conclusion it can be said that this work, performed with attention to detail and in all conscience, proves that emission free, highly efficient and eco-friendly air transport can be achieved, and even though the future of aviation might not look exactly like *RosE*, it surely will be stunning.

Exciting times lie ahead of us.

12. References

[1] IATA: "2036 Forecast Reveals Air Passengers Will Nearly Double to 7.8 Billion," 24.10.2017. [Online]. Available: http://www.iata.org/pressroom/pr/Pages/2017-10-24-01.aspx

[2] Europäisches Parlament; Generaldirektion Wissenschaft; Abteilung für Umwelt, Energie und Forschung, Stoa: "Umwelt und Luftverkehr," Themenpapier, No.2, p.5, 1998. [Online]. Available: https://www.hautsache.de/PDFs/Umweltverschmuz-Flug.pdf

[3] Bundesverband der deutschen Luftverkehrswirtschaft: "Informationen zum Thema Fluglärm," 2014. [Online]. Available: https://www.bdl.aero/download/1318/fakten-und-argumente-zum-thema-fluglarm-stand-juni-2014.pdf

[4] Khaki, A.M.; Forouhid, A.E.: "Noise Pollution around the Airport with Noise Exposure Forecasting Modeling," International Journal of Scientific and Research Publications, Vol.4, No.6, 2014.

[5] Umweltbundesamt: "Fluglärm Bericht 2017 des Bundesamtes," p.16, 2017. [Online]. Available: https://www.umweltbundesamt.de/sites/default/files/medien/1410/publikationen/2017-07-17_texte_56-2017_fluglaermbericht_v2.pdf

[6] CNBC: "Hyperloop is coming to Abu Dhabi by 2020," 28.05.2018. [Online]. Available: https://www.cnbc.com/2018/04/18/hyperloop-coming-to-abu-dhabi-by-2020.html

[7] Aircraft Commerce: "Owner's & Operators Guide: A330-200/-300," No.57, April/May 2008.

[8] DVZ Verkehrszeitung: "Airbus A330-200 Bestes Stueck der Airbus Bauer tritt seinen Dienst an," No. 059, 1998.

[9] Deutsche Lufthansa AG: "Lufthansa Balance. Daten und Fakten," Ed. 2003/2004.

[10] Airbus S.A.S.: "Special edition FAST. Flight Airworthiness Support Technology," Airbus technical magazine, October 2015.

[11] NASA: "X-48 Project Completes Flight Research for Cleaner, Quieter Aircraft," Release 13-105, 12.04.2013. [Online]. Available: https://www.nasa.gov/home/hqnews/2013/apr/HQ_13-105_X-48C_Final_Flight.html

[12] United Nations: "World Population Prospects, The 2015 Revision, Key Findings and Advance Tables," Department of Economic and Social Affairs, Population Division, New York, p.2, fig. 2, 2015.

[13] Hesselink, H.: "The Endless Runway Project," p.2, 2013.

[14] Hesselink, H.: "The Endless Runway Project – D5.4 Final Report," p.39, 2015.

[15] Chati, Y. S.; Balakrishnan, H.: "Analysis of Aircraft Fuel Burn and Emissions in the Landing and Take Off Cycle using Operational Data," 6th International Conference on Research in Air Transportation, Dep. Of Aeronautics and Astronautics, Massachusetts Institute of Technology, Cambridge, MA, USA, 2014.

[16] Rohacs, D.; Rohacs, J.: "Magnetic levitation assisted aircraft take-off and landing (feasibility study – GABRIEL concept)," Progress in Aerospace Sciences, No.85, 2016.

[17] Schach, R.; Jehle, P.; Naumann, R.: "Transrapid und Rad-Schiene-Hochgeschwindigkeitsbahn – Ein gesamtheitlicher Systemvergleich," p. 76, fig. 5.3, 2006.

[18] Airbus S.A.S.: "A330, Aircraft Characteristics, Airport and Maintenance Planning, AC," Customer Service, Technical Data Support and Service, January 2017.

[19] Schaedler, T.; Jacobsen, A.; Torrents, A.; Sorensen, A.; Lian, J.; Greer, J.; Valdevit, L.; Carter, W.: "Ultralight Metallic Microlattices," Science, Vol. 334, No.962, 2011. [Online]. Available: http://science.sciencemag.org/content/334/6058/962

[20] Westfield Technology Group: "Metallic Microlattice," [Online]. Available: https://westfieldavs.com/metallic-microlattice/

[21] MRO-Network: "What Passenger Cabin Windows Will Future Airliners Have?," Inside Mro, Maintenance, Repair & Overhaul, 27.11.2016. [Online]. Available: http://www.mro-network.com/maintenance-repair-overhaul/what-passenger-cabin-windows-will-future-airliners-have

[22] Raimondo, M.: "Improving the aircraft safety by advanced structures and protecting nanofillers," Ph.D., Dissertation, University of Salerno, 2014.

[23] Das, R.; Melchior, C.; Karumbaiah, K.: "Self-healing composites for aerospace applications," Advanced Composite Materials for Aerospace Engineering, p. 333-364, 2016;

[24] Blaiszik, B.; Kramer, S.; Olugebefola, S.; Moore, J.; Sottos, N.; White, S.: "Self-Healing Polymers and Composites," Annual Review of Materials Research, 2010.

[25] Norris, C.; Meadway, G.; O'Sullivan, M.; Bond, I.; Trask, R.: "Self-Healing Fibre Reinforced Composites via Bioinspired Vasculature," Advanced Functional Materials Journal, p. 6324-6333, 2011.

[26] Trask, R.; Williams, G.; Bond, I.: "Bioinspired self-healing of advanced composite structures using hollow glass fibres," Journal of the Royal Society, Interface 4, p. 363-371, 2007.

[27] Marino, M.; Siddique, O.; Sabatini, R.: "Benefits of the Blended Wing Body Aircraft Compared to Current Airliners," Conference: First International Symposium on Sustainable Aviation (ISSA 2015), Istanbul, Turkey, June 2015.

[28] Scholz, D.: "Empennage General Design," Aircraft Design, Lecture Notes, Chap. 9, Hamburg University of Applied Sciences, 2015.

[29] Rahn, A.: "Untersuchung der Realisierbarkeit und des Potentials eines Konzepts formveränderlicher Flügel basierend auf rotierenden Wellen zur Aktuierung," not published student research project, Institut für Luftfahrzeugtechnik, Technische Universität Dresden, 2017.

[30] Krishnan, K.; Bertram, O.; Seibel, O.: "Review of hybrid laminar flow control," Progress in Aerospace Sciences 93, p. 24-52, 2017.

[31] Torenbeek, E.: "Advanced Aircraft Design," John Wiley & Sons Ltd., 2013.

[32] Braslow, A.: "A history of suction type laminar-flow control with emphasis on flight research, monographs in aerospace history," NASA History Division, Vol. 13, 1999.

[33] Beck, N.; Landa, T.; Seitz, A.; Boermans, L.; Liu, Y.; Radespiel, R.: "Drag Reduction by Laminar Flow Control," *Energies,* 2018.

[34] Horn, M.: "Bauwesen und Fertigungskonzepte für Hybride Laminarerhaltung," DLRK Kongress, 2012.

[35] Young, T.; Humphreys, B.; Fielding, J.: "Investigation of hybrid laminar flow control (HLFC) surfaces," Aircraft Design, Vol. 4, p. 124-146, 2001.

[36] Risse, K.: "Preliminary Overall Aircraft Design with Hybrid Laminar Flow Control," Ph.D., Dissertation, Rheinisch-Westfällischen Technischen Hochschule, Aachen, 2016.

[37] Zhao, D-Y.; Huang, Z-P.; Wang, M-J.; Wang, T.; Jin, Y.: "Vacuum casting replication on shark skin for drag-reducing applications," Journal of Material Processing Technology 212, p. 198-202, 2012.

[38] Bechert, D.; Hage, W.: "Drag reduction with riblets in nature and engineering," Department of Turbulence Research, WIT Transactions on State of the Art of Science and Engineering, Vol. 4, 2006.

[39] Kordy, H.: "Process abilities of the riblet-coating process with dual-cure lacquers," CIRP, Journal of Manufacturing Science and Technology, Vol. 11, p. 1-9, 2018.

[40] Abbas, A.; de Vicente, J.; Valero, E.: "Aerodynamic technologies to improve aircraft performance," Aerospace Science and Technology 28, p. 100-132, 2013.

[41] Esker, B.; Wahls, R.: "ARMD Thrust 4: Transition to Low-Carbon Propulsion," Aeronautics R&T Roundtable, Washington DC, May 2016. [Online]. Available: https://www.nasa.gov/sites/default/files/atoms/files/armd-sip-thrust-4-508.pdf

[42] NASA Aeronautics: "Strategic Implementation Plan, 2017 Update," 2017.

[43] Bradley M.K.; Droney, C.K.: "Subsonic Ultra Green Aircraft Research: Phase II - Volume II - Hybrid Electric Design Exploration," 2015.

[44] Masson, P.; Luongo, C.: "High Power Density Superconducting Motor for All-Electric Aircraft Propulsion," IEEE Transaction on Applied Superconductivity, Vol. 15, p.4, 2005.

[45] Hoelzen, J.; Liu, Y.; Bensmann, B.; Winnefeld, C.; Elham, A.; Friedrichs, J.; Hanke-Rauschenbach, R.: "Conceptual Design of Operation Strategies for Hybrid Electric Aircraft," Energies, p.4, 16. January 2018.

[46] Masson, P.; Soban, D.; Upton, E.; Pienkos, J.; Luongo, C.: "HTS motors in aircraft propulsion: Design considerations," IEEE Trans. Appl. Supercond, vol. 15, p. 2218-2221, 2005.

[47] Fischer, G.; Hizsnyik, E.; Prieler, S.; Shah, M.; van Velthuizen, H.: "Biofuels and Food Security, Implications of an accelerated biofuels production," Summery of the OFID study, IIASA, Vienna, Austria, 2009. [Online]. Available: http://www.globalbioenergy.org/uploads/media/0903_OFID_-_BiofuelAndFoodSecurity.pdf

[48] Schulte, K.L.: "Elektroflug – Technologie, Geschichte und Zukunft," Köln, K.L.S. Publishing, p.52, 2014.

[49] Tan, P.; Jiang, H.R.; Zhu, X.B.; An, L.; Jung, C.Y.; Wu, M.C.; Shi, L.: "Advantages and challenges in lithium-air batteries," The Hong Kong University of Science and Technology, 2017. [Online]. Available: https://www.mae.ust.hk/~mezhao/pdf/317.pdf

[50] Vepa, R.: "Modeling and Dynamics of HTS Motors for Aircraft Electric Propulsion," aerospace, p.3, 2018.

[51] Dubensky, A.A.; Kovalev, K.L.; Larionoff, A.E.; Modestov, K.A.; Penkin, V.T.; Poltavets, V.N.: "An Outlook of the Use of Cryogenic Electric Machines Onboard Aircraft," IEEE Transactions on applied superconductivity, Vol. 26, No. 3, p. 1, April 2016.

[52] Berg, F.; Palmer, J.; Miller, P; Dodds, G.: "HTS System and Component Targets for a Distributed Aircraft Propulsion System," IEEE Transactions on applied superconductivity, 2017.

[53] Jones, C.E.; Norman, P.J.; Galloway, S.J.; Armstrong, M.J.; Bollman, A.M.: "Comparison of Candidate Architectures for Future Distributed Propulsion Aircraft," IEEE Transactions on applied superconductivity, Vol. 26, No. 6, September 2016.

[54] Berg, F.; Miller, J.P.P.; Husband, M.; Dodds, G.: "HTS Electrical System for a Distributed Propulsion Aircraft," IEEE Transactions on applied superconductivity, Vol. 25, No. 3, 2015.

[55] Luongo, C.A.; Masson, P.J.; Nam, T.; Mavris, D.; Kim, H.D.; Brown, G.V.; Waters, M.; Hall, D.: "Next generation more-electric aircraft: A potential application for HTS superconductors," IEEE Transactions on Applied Superconductivity, Vol. 19, No. 3, 2009.

[56] Winnefeld, C.; Kadyk, T.; Bensmann, B.; Krewer, U.; Hanke-Rauschenbach, R.: "Modelling and Designing Cryogenic Hydrogen Tanks for Future Aircraft Applications," Energies, 2018.

[57] Linde AG: "The Driving Force," [Online]. Available: https://www.the-linde-group.com/internet.global.thelindegroup.global/en/images/00299_LG_Wasserstoff_Broschuere_218x305_EN14_233488.pdf?v=1.0. [Accessed 23 6 2018]

[58] Mital, S.; Gyekenyesi, J.; Arnold, S.; Sullivan, R.; Manderscheid, J.: "Review of Current State of the Art and Key Design Issues with Potential Solutions for Liquid Hydrogen Cryogenic Storage Tank Structures for Aircraft Applications," National Aeronautics and Space Administration, Cleveland, OH, USA, 2006.

[59] Brewer, G.D.: "Hydrogen Aircraft Technology," Boca Raton, FL, USA: CRC Press, 1991.

[60] Armstrong, M.; Blackwelder, M.; Bollman, A.; Ross, C.; Campbell, A.; Jones, C.; Norman, P.: "Architecture, Voltage, and Components for a Turboelectric Distributed Propulsion Electric Grid," 2015.

[61] Zon, N. v.: "Liquid Hydrogen Powered Commercial Aircraft," Technical University of Delft, 2012.

[62] Wolf, K.: "Flugleistungen," Luftfahrzeugauslegung, Lecture notes, Lehrstuhl für Luftfahrzeugtechnik, Institut für Luft- und Raumfahrttechnik, Technische Universität Dresden, 2015.

[63] Airbus S.A.S: "Aircraft Characteristics, Airport and Maintenance Planning," Blagnac Cedex, France, 2017.

[64] European Aviation Safety Agency: "Type-Certificate Data Sheet RB211 Trent 700 Series Engine," 2013.

[65] Schiktanz, D.; Scholz, D.: "Box Wing Fundamentals - An Aircraft Design Perspective," Hamburg University of Applied Sciences, Hamburg, 2011.

[66] Aceves, S.; Petitpas, G.; Switzer, V.: "Rapid High Pressure LH2 Refuelling for Maximum Range and Dormancy," Lawrence Livermore National Laboratory, 2014.

[67] European Aviation Safety Agency: "Certification Specifications and Acceptable Means of Compliance for Large Aeroplanes," CS-25, Amendment 18, Appendix J, 2016.

[68] International Civil Aviation Organization: "Airport Air Quality Manual – First Edition," 3-A1-30, 2011.

[69] Jenkinson, L.; Simpkin, P.; Rhodes, D.: "Civil Jet Aircraft Design," 1999.

[70] Wolf, K.: Excel-Programm zur Berechnung von Operational Empty Weight, not published Excel file, Institut für Luftfahrzeugtechnik, Technische Universität Dresden, 2015.

13. List of Figures

14. List of Tables

15. Appendix

Appendix A1

Appendix A2

Performance data		A330-200			
			characteristics of Air		
Flight altitude	H	39000 ft	adiabatic koeff.	κ	1,4
		11887,2 m	kin. Viscosity	v	3,78E-05 at 35000ft**
Air density in height H*	ρ	0,3243 kg/m^3	gas constant	R	287,05 J/kg*K
Mach number	M	0,82			
Temperature in height H*		210,88 K	*for values of -5000 to 11000m and 20000 to 32000m		
		-62,2668 °C	**acc. to ISA		
Cruise velocity	v	238,71 m/s			
Max Take-off weight	m_{MTO}	233000 kg			
Lift at cruise velocity	c_L	0,6842	$f(m, \rho, v, S_F)$		

Wings			
Wing area	S_W	361,60 m²	
Wingspan	b	60,30 m	
Aspect ratio	Λ	10,06	
Angle	φ	30 °	0,51836279 rad
Wetted area	$S_{W,Wet}$	736,42 m²	$f(S_L, \delta_m)$
Wing depth at root	l_R	10,55 m	
Wing thickness at root	d_R	1,70 m	
rel. Wing thickness at root	$\delta_{m,R}$	0,1611	
Wing depth at tip	l_T	2,48 m	
Wing thickness at tip	d_T	0,29 m	
rel. Wing thickness at tip	$\delta_{m,T}$	0,1169	
char. Length	l_W	6,52 m	$f(l\_W, l\_S)$
median rel. Wing thickness	δ_m	0,1280	
Tapering	λ	0,2351	
Oswald factor	e	0,8350	

Fuselage			
Length	l_F	57,51 m	
Diameter	d_F	5,64 m	
Cross section area	$S_{Q,F}$	24,98 m²	
wetted area	$S_{F,Wet}$	827,01 m²	$f(l_R, S_{Q,R}, \lambda_R)$

Empennage			
Empennage area	S_E	55,00 m²	
char. Length	l_E	4,23 m	
median rel. Thickness	δ_m	0,10	
Angle	φ	33 °	0,57595865 rad
wetted area	$S_{E,Wet}$	111,21 m²	$f(S_L, \delta_m)$

engine nacells			
engine length	l_{TW}	3,9120 m	
engine diameter	d_{TW}	2,4740 m	
wetted area	$S_{TW,Wet}$	30,4052	

Calculation of drag

Parasite drag coeff.	c_{D0}	0,0127

$$C_{W_0} = \frac{1}{S_F} \sum_k \left[c_f \, k_F \, k_i \, S_{wet} \right]_k + \sum_n \left[\Delta C_{W_0} \right]_n \qquad c_{W0} = c_{D0}$$

$\hookrightarrow$ Flügelfläche

Wing			
Form factor	$k_{F,W}$	1,0100	$f(\delta_m, \phi)$
Interference faktor	$k_{i,W}$	1,00	for low-wing aircraft with fairing-covered wing-fuselage transition
Reynolds number	Re_W	41143408	$f(V, l_W, v)$
Friction coefficient of Surface	c_f	0,0026	$f(l)$ Assumption: turbulent boundary layer;
Parasite drag	c_{D0}	0,0053	surface coated with paint
Additional drag	Δc_{D0}	0,0003	

Empennage

Form factor	$k_{F,E}$	1,3522	$f(\delta_m, \phi)$
Interference faktor	$k_{i,E}$	1,05	conventional empennage
Reynolds number	Re_E	26713218	$f(V, l_W, v)$
Friction coefficient of Surface	c_f	0,0028	$f(I)$ Assumption: turbulent boundary layer;
Parasite drag	c_{D0}	0,0012	surface coated with paint
Additional drag	Δc_{D0}	0,0001	

Fuselage

Form factor	$k_{F,F}$	1,1038	$f(\lambda_F)$
Interference factor	$k_{i,F}$	1,00	
Factor	λ_F	10,1968	$f(l_F, S_{Q,F})$
Reynolds number	Re_F	363186089	$f(V, l_W, v)$
Friction coefficient of Surface	c_f	0,0019	$f(I)$ Assumption: turbulent boundary layer;
Parasite drag	c_{D0}	0,0047	surface coated with paint
Additional drag	Δc_{D0}	0,0003	
Additional drag through cockpit windows		0,0001	

engine nacells

Form factor	$k_{F,TW}$	1,2213
Factor	λ_{TW}	1,5812
interference factor	$k_{i,TW}$	1,1000
Friction coefficient of Surface	$c_{f,TW}$	0,0028
Parasite drag	$c_{D0,TW}$	0,0003

Induced drag coefficient	c_{Di}	**0,0183**

Induced Drag
- Oswald Factor -

- Induced Drag of the Aircraft
$$C_{W_i} = \frac{1}{\pi \Lambda e_{AC}} C_A^2$$

- Oswald-Faktor mit Rumpf-Einfluss
$$e_{AC} = k_{Fuselage}\, e_{Wing}$$
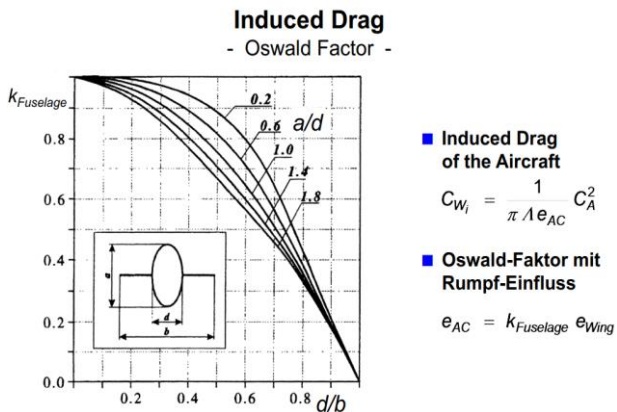
	d/b	0,0935
	$k_{Fuselage}$	0,97

Overall drag coefficient	c_D	**0,0310**

ANNOTATION: Wave drag has been neglected due to relatively low effects for Ma<0,85

Thrust

$$T = \rho/2 * c_W * S_F * v^2$$

required thrust	$T_{req,A330}$	103655 N	103,7 kN
start thrust	T_0	316000 N	
factor $T_0/T_{req,A330}$	f_T	3,05	

Power and Energy

required propulsive power	P_{req}	24743826 J/s	$f(F_{req}, v)$

fuel mass for cruise

max. zero fuel weight	m_{ZF}	168000 kg	from Airbus datasheet
fuel at take-off	$m_{F,TO}$	65000 kg	$f(m_{MTO}, m_{ZF})$
fuelburn taxiing	Δm_{Taxi}	473 kg	
fuelburn LTO	Δm_{LTO}	2230 kg	
fuel for cruise	$m_{F,Cruise}$	62297 kg	

Energy

specific energy of Kerosene	$e_{Kerosene}$	43300000 J/kg	43,3 MJ/kg	
energy stored in tank for cruise	$E_{Tank,Cruise}$	**2,69746E+12 J**	**2697 GJ**	
approximated part of energy used for cabin, a	f_L	0,1		
efficiency of gas turbine	$\eta_{Turbine}$	0,5		
Energy remaining for propulsion	$E_{prop,A330}$	1,09247E+12 J	1092 GJ	$f(E_{Tank}, \eta_{Turbine})$
flight time at P_{req} for $E_{prop,A330}$	t_{cruise}	44151,26992 s	12 h	$f(E_{prop,A330}, P_{req})$
flight distance	s_{Cruise}	10539520,11 m	10540 km	$f(t_{cruise}, v)$

Start: ground run + climb to 1500ft at 250kts

available thrust for start	T_0	316000 N		
maximum lift coeff.	$c_{L,max}$	1,98		Assumption: similar levels of thrust needed
take-off speed	v_{TO}	72,20 m/s		in climb for both aircraft,
time while under start thrust	t_{Start}	1 m	60 s	therefore neglected
height at segment end	h_E	1500 ft	457,2 m	
velocity at segment end	v_E	250 kts	128,6 m/s	
required energy for segment	$E_{req,TO}$	**6695364351 J**	**7 GJ**	$f(T_0, t_{Start}, v, \eta_{Turbine})$

Climb to 35000ft at 310kts

height at segment end	h_E	35000 ft	10668 m	
velocity at segment end	v_E	310 kts	159,464 m/s	
required energy for segment	$E_{req,Climb}$	**30967392951 J**	**31 GJ**	$f(t_{Start}, v, \eta_{Turbine})$
total energy needed for start - climb - cruise	$E_{req,totsl}$	**2,73512E+12 J**	**2735 GJ**	

Appendix A3

Performanca data		RosE				
				characteristics of Air		
Flight altitude	H	45000	ft	adiabatic koeff	κ	1,4
		13716	m	kin. Viscosity	ν	3,78E-05 at 35000ft**
Air density in height H*	ρ	0,2533	kg/m^3	gas constant	R	287,05 J/kg*K
Mach number	M	0,75				
Temperature in height H*	T	199,00	K	*for values of -5000 to 11000m and 20000 to 32000m		
		-74,154	°C	**acc. to ISA		
Cruise velocity	v	212,09	m/s			
Max Take-off weight	m_{MTO}	154000	kg			
Lift at cruise velocity	c_L	0,6524		$f(m, \rho, v, S_F)$		

Lower Wings

Wing area	S_W	212,10	m^2	
Wingspan	b	52,20	m	
Aspect ratio	Λ	12,85		
Angle	ϕ	23	°	0,401425728 rad
Wetted area	$S_{W,Wet}$	435,12	m^2	$f(S_L, \delta_m)$
Wing depth at root	l_R	15,39	m	
Wing thickness at root	d_R	2,73	m	
rel. Wing thickness at root	$\delta_{m,R}$	0,1774		
Wing depth at tip	l_T	2,07	m	
Wing thickness at tip	d_T	0,31	m	
rel. Wing thickness at tip	$\delta_{m,T}$	0,1498		
char. Length	l_W	8,73		$f(l\_W, l\_S)$
median rel. Wing thickness	δ_m	0,1567		
Tapering	λ	0,1345		
Oswald factor	e	0,8294		

Upper Wings

Wing area	S_W	194,40	m^2	
Wingspan	b	52,20	m	
Aspect ratio	Λ	14,02		
Angle	ϕ	10	°	
Wetted area	$S_{W,Wet}$	393,62	m^2	
Wing depth at root	l_R	6,28	m	
Wing thickness at root	d_R	0,30	m	
rel. Wing thickness at root	$\delta_{m,R}$	0,0478		
Wing depth at tip	l_T	2,07	m	
Wing thickness at tip	d_T	0,26	m	
rel. Wing thickness at tip	$\delta_{m,T}$	0,1246		
char. Length	l_W	4,18		
median rel. Wing thickness	δ_m	0,1054		
Tapering	λ	0,3296		
Oswald factor	e	0,8281		
Combined wing area	$S_{W,Total}$	**406,50**	m^2	

Fuselage

Length	l_F	57,51	m	
Diameter	d_F	5,64	m	
Cross section area	$S_{Q,F}$	24,98		
wetted area	$S_{F,Wet}$	827,01	m^2	$f(l_R, S_{Q,R}, \lambda_R)$

Empennage

Empennage area	S_E	43,85	m^2	
char. Length	l_E	5,79	m	
median rel. Thickness	δ_m	0,05		
Angle	ϕ	40	°	0,698131701 rad
wetted area	$S_{E,Wet}$	87,52	m^2	$f(S_L, \delta_m)$

Calculation of drag

| Parasite drag coeff. | c_{D0} | **0,0179** | deviation from base | 40,6 % |

$$C_{W_0} = \frac{1}{S_F} \sum_k \left[c_f \, k_F \, k_i \, S_{wet} \right]_k + \sum_n \left[\Delta C_{W_0} \right]_n$$

→ Flügelfläche $c_{w0} = c_{D0}$

Lower Wing

Form factor	$k_{F,W}$	1,1762	$f(\delta_m, \phi)$	
Interference faktor	$k_{i,W}$	1,00	for low-wing aircraft with fairing-covered wing-fuselage transition	
Reynolds number	Re_W	48983372	$f(V, l_W, v)$	
Friction coefficient of Surface	c_f	0,0025	$f(l)$	Assumption: turbulent boundary layer;
Parasite drag	c_{D0}	0,0060		surface coated with paint
Additional drag	Δc_{D0}	0,0004		

Upper Wing

Form factor	$k_{F,W}$	1,2671	$f(\delta_m, \phi)$	
Interference faktor	$k_{i,W}$	1,00	for up-wing aircraft with fairing-covered wing-fuselage transition	
Reynolds number	Re_W	23425610	$f(V, l_W, v)$	
Friction coefficient of Surface	c_f	0,0028	$f(l)$	Assumption: turbulent boundary layer;
Parasite drag	c_{D0}	0,0072		surface coated with paint
Additional drag	Δc_{D0}	0,0004		

Empennage

Form factor	$k_{F,E}$	1,6208	$f(\delta_m, \phi)$	
Interference faktor	$k_{i,E}$	1,03	für V-Leitwerk	
Reynolds number	Re_E	32487253	$f(V, l_W, v)$	
Friction coefficient of Surface	c_f	0,0026	$f(l)$	Assumption: turbulent boundary layer;
Parasite drag	c_{D0}	0,0010		surface coated with paint
Additional drag	Δc_{D0}	0,0001		

Fuselage

Form factor	$k_{F,F}$	1,1038	$f(\lambda_F)$	
Interference faktor	$k_{i,F}$	1,00		
Factor	λ_F	10,20	$f(l_F, S_{Q,F})$	
Reynolds number	Re_F	322684272	$f(V, l_W, v)$	
Friction coefficient of Surface	c_f	0,0019	$f(l)$	Assumption: turbulent boundary layer;
Parasite drag	c_{D0}	0,0042		surface coated with paint
Additional drag	Δc_{D0}	0,0003		

Additional drag through cockpit windows		8,37E-05
Reduction of drag through Sharksin	$\Delta c_{D0,Skin}$	0,0008
Reduction of drag through HLFC	$\Delta c_{W,HLFC}$	0,0008

| Induced drag coefficient | c_{Di} | **0,006113141** | deviation from base | -66,6 % |

Induced Drag
- Oswald Factor -

$k_{Fuselage}$, a/d 0.2, 0.6, 1.0, 1.4, 1.8, d/b

- Induced Drag of the Aircraft

$$C_{W_i} = \frac{1}{\pi \, \Lambda \, e_{AC}} \, C_A^2$$

- Oswald-Faktor mit Rumpf-Einfluss

$$e_{AC} = k_{Fuselage} \, e_{Wing}$$
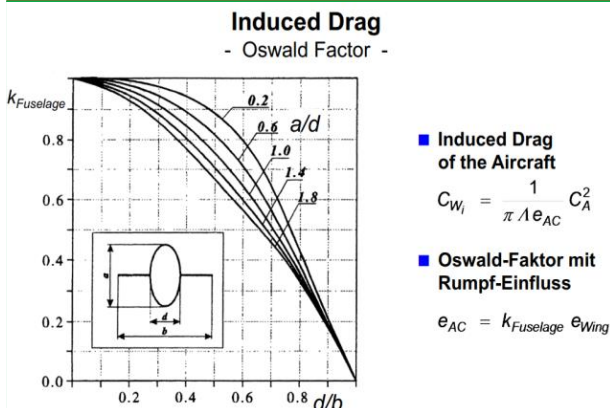
	d/b	0,1080
	$k_{Fuselage}$	0,96
induced drag of standard configuration	$c_{Di,Standard}$	0,013243934

Reduction through Boxwing configuration

Height of Boxwing configuration	h_{BW}	2,64	m
Height-to-span-ratio	h/b	0,050574713	
induced drag of Boxwing configuration	c_{Di}	0,006113141	

$$(18)\quad \frac{D_{i,box}}{D_{i,ref}} = \frac{0,44 + 0,9594 \cdot h/b}{0,44 + 2,219 \cdot h/b}.$$

from D.Schiktanz; D. Scholz; "Box Wing Fundamentals - An Aircraft Design Perspective"

Overall drag coefficient	c_D	**0,0240**	deviation from base	-22,6 %

ANNOTATION: Wave drag has been neglected due to relatively low effects for Ma<0,85

L/D Ratio E **27,1657**

max.-L/D drag coeff.	$c_{D,Emax}$	0,0358
max.-L/D lift coeff.	$c_{L,Emax}$	0,7741
max. L/D ratio	E_{max}	21,62
optimal L/D ratio	E_{opt}	18,72

Thrust

$$T=W=\rho/2 \cdot c_W \cdot S_F \cdot v^2$$

required thrust	T_{req}	55612 N	55,6 kN
required take-off thrust	$T_{req,0}$	144107 N	

Power and Energy

required propulsive power	P_{req}	11794931 J/s	$f(F_{req}, v)$
required take-off power	$P_{req,0}$	18445734 J/s	
flight time at P_{req} for s_{Cruise}	t_{cruise}	49692,93027 s	14 h $\quad f(s_{Cruise}, P_{req})$
efficiency of HTS Motors	η_{HTS}	0,995	
efficiency of fuel cells	η_{fc}	0,85	
efficiency of propeller	η_{prop}	0,90	
energy stored in tank for cruise	$E_{Tank,Cruise}$	8,55585E+11 J	856 GJ $\quad$ -68,3

Energy

approximated part of energy used for cabin, avioni	f_L	0,1	
Energy remaining for propulsion	$E_{prop,A330}$	7,66176E+11 J	766 GJ $\quad f(E_{Tank}, \eta_{Turbine})$

Start: ground run + climb to 1500ft at 250kts

height at segment end	h	1500 ft	457,2 m
velocity at segment end	v	250 kts	128,6 m/s
required energy for segment	$E_{req,TO}$	2363680302 J	2,36 GJ $\quad f(T_0, t_{Start}, v, \eta_{Turbine})$ $\quad$ -64,7

Climb to 45000ft at 310kts

height at segment end	h	45000 ft	13716 m
velocity at segment end	v	310 kts	159,464 m/s
required energy for segment	$E_{req,Climb}$	23293668472 J	23 GJ $\quad f(t_{Start}, v, \eta_{Turbine})$ $\quad$ -24,8
Energy reduction from reduced drag	ΔE_{Drag}	-5798818736 J	-6 GJ
total energy needed for start - climb - cruise	$E_{req,total}$	8,75443E+11 J	875 GJ

deviation from base: **-68,0** %

Appendix A4

Energy supply			
specific power fuel cell	p_{FC}	2000 W/kg	
required take-off power	$P_{req,0}$	18445734 W	see "RosE"
Weight of required fuel cells	$m_{req,FC}$	9223 kg	
Propulsion			
specific power HTS motor	p_{HTS}	25000 W/kg	
required take-off power	$P_{req,0}$	18445734 W	see "RosE"
Weight of required motors	$m_{req,HTS}$	738 kg	
Fuel			
specific energy LH2	e_{LH2}	119900000 J/kg	119,9 MJ/kg
required energy for mission	$E_{req,total}$	8,75443E+11 J	see "RosE"
fuel mass from energy	m_{LH2}	7301 kg	
boil-off/day	Δm_{LH2}	0,03	
fuel mass for mission	$m_{req,LH2}$	7527 kg	
Tanks			
mass factor tanks	η_{Tank}	0,64 f(tank geometry)	
mass of tanks	m_{Tanks}	3881 kg	

Other weights:	A330-200	RosE	Factor	
Operational Items:	**4329 kg**	**4329 kg**		
crew	1040 kg	1040 kg	1	
consumables	2783 kg	2783 kg	1	
safety equipment	506 kg	506 kg	1	
Structural weight	**87058 kg**	**70636 kg**		remarks
wings	37091 kg	44509 kg	1,2	1
fuselage	32841 kg	19705 kg	0,6	2
empennage	3435 kg	2748 kg	0,8	3
landing gear	9902 kg	2674 kg	0,27	4
engine installation	3788 kg	0 kg	0	
emergency landing skid	0 kg	1000 kg	1	5
Propulsion	**15217 kg**	**16165 kg**		
motors	11596 kg	738 kg		6
thrust reversal	2114 kg	0 kg		7
subsystems	642 kg	963 kg	1,5	8
fuel system	865 kg	1297 kg	1,5	9
fuel cells	0 kg	9223 kg		10
tank	0 kg	3944 kg		10
Equipment	**22291 kg**	**18325 kg**		
ECS	2395 kg	3592 kg	1,5	11
hydraulics & pneumatics	1974 kg	0 kg	0	12
electric	2048 kg	4095 kg	2	
APU	783 kg	0 kg	0	13
flight control	2855 kg	1999 kg	0,7	14
avionic	1657 kg	1657 kg	1	
interior	10580 kg	6982 kg	0,66	15
operational empty weight	**128895 kg**	**109455 kg**		
	100 %	-17,8 %		
max zero fuel weight	168000 kg	148560 kg		
payload	39105 kg	39105 kg	1	
fuel at maximum payload	65000 kg	7527 kg	-88,42	
maximum take-off weight	**233000 kg**	**156087 kg**		
	100 %	-33,0 %		

1 zusätzliche Struktur (Erweiterung Flügelkasten, Flügel etwas kürzer, hinterer Flügel schmaler), aber oberer Flügel

2 A330 Rumpf bleibt gleich, Verwendung von FVW, keine Fenster, weniger von Nietverbindungen (Klebeverbindungen)

3 Seitenleitwerk entfällt

4 Gewicht verringert sich wegen entfallendem Fahrwerk

5 Kufen sind Teile des Rumpfes, die im Bedarfsfall ausgefahren werden

6 s.o. (Berechnung)

7 Schubumkehr mit Elektromotor realisiert

8 Kühlung, Transport zur Brennstoffzelle

9 aus der selbsterstellten Berechnung

10 s.o. (Berechnung)

11 Gewicht von Kompressoren im Vergleich zu Pneumatik

12 Hydraulik abgeschafft

13 keine APU mehr

14 fly-by-light

15 micro lattice